AFRL-RW-EG-TR-2010-106

Controlled Loading Fragmentation: Experiments and Continuum Damage Modeling

D. E. Lambert
J. Weiderhold

Air Force Research Laboratory, Munitions Directorate
AFRL/RWMW
101 W. Eglin Blvd
Eglin AFB, FL 32542-6810

M. V. Hopson

Naval Surface Warfare Center
Dahlgren Division
Dahlgren, VA 22448

J. Osborn
General Dynamics-Ordnance and Tactical Systems
Niceville, FL 32578

Jul 2010

Interim Report for Period Oct 2008 – Jul 2010

AIR FORCE RESEARCH LABORATORY
MUNITIONS DIRECTORATE

■ **Air Force Materiel Command** ■ **United States Air Force** ■ **Eglin Air Force Base, FL 32542**

NOTICE AND SIGNATURE PAGE

Using Government drawings, specifications, or other data included in this document for any purpose other than Government procurement does not in any obligate the U.S. Government. The fact that the Government formulated or supplied the drawings, specifications, or other data does not license the holder or any other person or corporation, or convey any rights or permission to manufacture, use, or sell any patented invention that may relate to them.

Qualified requestors may obtain copies of this report from the Defense Technical Information Center (DTIC) (http://www.dtic.mil).

AFRL-RW-EG-TR-2010-106 HAS BEEN REVIEWED AND IS APPROVED FOR PUBLICATION IN ACCORDANCE WITH ASSIGNED DISTRIBUTION STATEMENT.

FOR THE DIRECTOR:

//Original Signed//	//Original Signed//	//Original Signed//
HOWARD G. WHITE	MATTHEW J. MATYAC	DAVID E. LAMBERT
Technical Advisor	Technical Advisor	Program Manager
Ordnance Division	Damage Mechanisms Branch	Damage Mechanisms Branch

This report is published in the interest of scientific and technical information exchange, and its publication does not constitute the Government's approval or disapproval of its ideas or findings.

REPORT DOCUMENTATION PAGE

Form Approved
OMB No. 0704-0188

1. REPORT DATE *(DD-MM-YYYY)*	**2. REPORT TYPE**	**3. DATES COVERED** *(From - To)*
Jul 2010	Interim	Oct 2008 – Jul 2010

4. TITLE AND SUBTITLE

Controlled Loading Fragmentation: Experiments and Continuum Damage Modeling

5a. CONTRACT NUMBER

5b. GRANT NUMBER

5c. PROGRAM ELEMENT NUMBER
62602F

6. AUTHOR(S)
(1) Dr. David E. Lambert
(1) 1Lt. Joseph Weiderhold
(2) Michael V. Hopson
(3) John Osborn

5d. PROJECT NUMBER
2502

5e. TASK NUMBER
12

5f. WORK UNIT NUMBER
99

7. PERFORMING ORGANIZATION NAME(S) AND ADDRESS(ES)
(1) Air Force Research Laboratory
Munitions Directorate
101 W. Eglin Blvd., Ste. 135
Eglin Air Force Base, Florida 32542-6810
(2) Naval Surface Warfare Center
Dahlgren Division, Dahlgren VA 22448
(3) General Dynamics- OTS
Niceville, FL 32578

8. PERFORMING ORGANIZATION REPORT NUMBER

9. SPONSORING / MONITORING AGENCY NAME(S) AND ADDRESS(ES)
Air Force Research Laboratory
Munitions Directorate, AFRL/RWMW
101 W. Eglin Blvd., Ste. 135
Eglin AFB FL 32542-6810

10. SPONSOR/MONITOR'S ACRONYM(S)
AFRL-RW-EG

11. SPONSOR/MONITOR'S REPORT NUMBER(S)
AFRL-RW-EG-TR-2010-106

12. DISTRIBUTION / AVAILABILITY STATEMENT
DISTRIBUTION A. Approved for Public Release; Distribution Unlimited. 96th ABW/PA Approval and Clearance # 96 ABW-2010-0591, 24 November 2010.

13. SUPPLEMENTARY NOTES

14. ABSTRACT Fragmentation of metals due to high strain rate loading is a relevant topic for explosively driven metals, high velocity impacts and other energetic material scenarios. The ability to perform relevant and well-controlled experiments is a challenge. The ability to predictively model such failure and fragmentation events in dynamic continuum mechanics codes, or „hydrocodes", is even more of a challenge. A collection of three papers are presented on the design, analysis and experiments of an explosively driven cylinder fragmentation event. The first paper describes the background of the problem and provides details of an explosively loaded cylinder geometry that establishes either plane strain or uniaxial stress conditions for failure. Parametric variations of cylinder material, initiation configuration, and cylinder dimensions are addressed. The results of this initial paper are then used to manufacture items and conduct physical experiments, which are reported in the second paper. Experiments of free-air expansion and water-recovery are conducted to extract all necessary engineering measures from which to calibrate and utilize the Johnson-Cook damage model. Experimental data obtained includes the strain –to-failure, strain-rate, fragment velocity, fragment mass, mass distributions, size distributions and approximate time of fragmentation. Diagnostics of photonic Doppler velocimetry and ultra-high speed framing cameras provide a coupled data set for high-confidence and meaningful input to the model. The last paper takes the experiment data and invokes a Weibull compensated Johnson-Cook model to explicitly calculate fragment distributions. These distributions are compared with that actually recovered . Additionally, perturbations and insight to limitations of the Eulerian and Lagrangian approaches to modeling are made with conclusions providing a state-of-the capability for predictive design capability.

15. SUBJECT TERMS
Munitions fragmentation, continuum damage modeling, Johnson-Cook damage model, explosive fragmentation

16. SECURITY CLASSIFICATION OF:			**17. LIMITATION OF ABSTRACT**	**18. NUMBER OF PAGES**	**19a. NAME OF RESPONSIBLE PERSON**
a. REPORT	**b. ABSTRACT**	**c. THIS PAGE**			David E. Lambert
UNCLASSIFIED	UNCLASSIFIED	UNCLASSIFIED	UL	52	**19b. TELEPHONE NUMBER** *(include area code)* (850) 882-7991

Table of Contents

Contents

Table of Figures

Chapter 1

Chapter 2

Chapter 3

Preface

This report is the result of a very interactive collaboration between the Air Force Research Laboratory, Lawrence Livermore National Laboratory, and the Naval Surface Warfare Center in Dahlgren, VA. AFRL/RW had begun in-house exploits along the area of controlled fragmentation of explosively loaded cylinders and used the innovative predecessor research of Dr. Dana Goto, Dr. Ted Orzechowski, and Dr. Keo Springer of LLNL as a sound basis from which to begin. The experiments of the LLNL were used as a benchmark method to begin in-house experiments with materials of AFRL/RW interest. 1Lt. Joseph Weiderhold of AFRL/RWMW provided direction and excellent oversight of the experiments. They were conducted at the Advanced Warheads Experimentation Facility (AWEF) with the superb technical support of the range crew under Ms. Brenda Weekley's leadership. Along the technical path, Mr. Michael Hopson of the NSWC-Dahlgren joined the research team as an invaluable member having the ability to incorporate the experimental results into the statistically-driven damage functions. Mr. Hopson continued with extensive probing and inquisition of the numerically-induced artifacts and errors of this problem. Dr. David Lambert managed the technical efforts, provided the interactive collaborations between the research groups, oversaw the computational efforts by John Osborn, General Dynamics-OTS and performed analysis of the data to get comprehensible research results. The three papers were presented at the 2010 American Society of Mechanical Engineers, Pressure Vessels and Piping Conference held in Bellevue, WA in July 2010. This technical report is basically comprised of those three papers to provide a logical summation and reporting point of this effort. This report may also serve as the final report of this dynamic fragmentation effort of JON 25021299 if fiscal year 2011 (FY2011) increment does not get funded.

.

Abstract

Fragmentation of metals due to high strain rate loading is a relevant topic for explosively driven metals, high velocity impacts and other energetic material scenarios. The ability to perform relevant and well-controlled experiments is a challenge. The ability to predictively model such failure and fragmentation events in dynamic continuum mechanics codes, or 'hydrocodes', is even more of a challenge. A collection of three papers are presented on the design, analysis and experiments of an explosively driven cylinder fragmentation event. The first paper describes the background of the problem and provides details of an explosively loaded cylinder geometry that establishes either plane strain or uniaxial stress conditions for failure. Parametric variations of cylinder material, initiation configuration, and cylinder dimensions are addressed. The results of this initial paper are then used to manufacture items and conduct physical experiments, which are reported in the second paper. Experiments of free-air expansion and water-recovery are conducted to extract all necessary engineering measures from which to calibrate and utilize the Johnson-Cook damage model. Experimental data obtained includes the strain –to-failure, strain-rate, fragment velocity, fragment mass, mass distributions, size distributions and approximate time of fragmentation. Diagnostics of photonic Doppler velocimetry and ultra-high speed framing cameras provide a coupled data set for high-confidence and meaningful input to the model. The last paper takes the experiment data and invokes a Weibull compensated Johnson-Cook model to explicitly calculate fragment distributions. These distributions are compared with that actually recovered. Additionally, perturbations and insight to limitations of the Eulerian and Lagrangian approaches to modeling are made with conclusions providing a state-of-the capability for predictive design capability.

CHAPTER 1

Proceedings of the 2010 Pressure Vessels and Piping Conference

PVP-2010

July 18-22, 2010, Bellevue, Washington

Paper PVP2010-25051

Dynamic Fragmentation Experiments Under Plane Strain and Uniaxial Stress Conditions

David E. Lambert
Air Force Research Laboratory/Munitions Directorate
Eglin Air Force Base, FL, USA

1st Lt. Joseph Weiderhold
Air Force Research Laboratory/Munitions Directorate
Eglin Air Force Base, FL, USA

John Osborn
General Dynamics-Ordnance & Tactical Systems
Niceville, FL,USA

Michael V. Hopson
Naval Surface Warfare Center, Dahlgren Division
Dahlgren, VA, USA

ABSTRACT

The explosively loaded cylinder is further studied as an experimental method to improve dynamic fracture and fragmentation modeling. Details of the cylinder configuration are investigated to prescribe controlled loading conditions of uniaxial stress and plane strain. Commonly used fracture models, e.g. Johnson-Cook, are calibrated with strain at fracture under such controlled conditions. Earlier works by Goto, et al [1] had used thin-walled tubes to provide plane strain loading and shorter "rings" to establish uniaxial stress conditions. This paper extends on that work to look at alternative cylinder dimensions and metals of interest. A tungsten alloy, Aero 224, and a high strength steel, Eglin Steel (ES-1), are the subject metals. Dynamic, continuum-mechanics based modeling and simulations evaluated whether the stress triaxiality conditions are being met as design parameters of cylinder wall-thickness, explosive type, and initiation configuration. Experiments conducted for this effort, reported in greater detail by Weiderhold [2], provided precise measurement of the cylinder expansion process and fragmentation distributions.

An explosively driven metal event is usually considered highly transient and multi-dimensional in stress; however, selective design of the system can result in a controlled experimental configuration. The analysis shows that the ductile ES-1 steel cylinder and rings do establish the desired plane strain and uniaxial stress conditions, respectively, as the cylinder expands to failure. Ultra-high speed photography

experiments verify the time of fracture and correlate casewall expansion and velocity measurements. The analysis of the tungsten alloy had verified that if the material was capable of achieving at least a 25% strain to failure then the cylinder and rings would be viable controlled loading paths. However, fragments recovered from the explosively driven rings verified that the strain to failure was less than 14% and the triaxiality condition of uniaxial stress was not achieved by then. The data of this fragmentation under controlled loading conditions are to be used to determine coefficients for fracture-models and serve as benchmarks of relevant, dynamic fragmentation processes for future explosive/metal design opportunities.

INTRODUCTION

Computational continuum design codes have made significant advancements in modeling capability, but they still lack a robust, predictive capability in fracture and fragmentation. This is true for even some of the simplest explosive-metal designs in history; the canon ball or the pipe-bomb. The limitation is primarily the result of codes having homogeneous property descriptions while real materials have heterogeneous microstructures that fracture through void nucleation, growth and coalescence. The statistically compensated fracture model is one way to bridge this connection between the stochastic processes of real material fragmentation and that of continuum modeling. The models, however, need parameter calibration under controlled loading conditions and representative strain, strain-rate, and temperature domains. Many classical high-rate mechanical test devices (i.e. split-Hopkinson pressure bar, Taylor cylinder impact) achieve controlled loading conditions but still lack the initial shock loading event from the detonation wave. The work of Goto et al [1] was a systematic approach to exploiting the explosively driven cylinder as not just an application relevant, fragmenting pipe-bomb, but as a dynamic test apparatus for controlled loading studies. Their work resulted in a calibration of the generalized Johnson-Cook fracture model [3]. Therefore, one can establish a calibrated fracture model that can be compensated via probability distribution functions to mimic the stochastic response in heterogeneous material properties. This process was demonstrated with promising results for AerMet100 steel using a Weibull statistical distribution of the initial failure strain [4].

CYLINDER DESIGN

An axisymmetric cylindrical geometry is used with explosive core diameter of 5.08cm (2.0in). The metallic tube thickness was chosen using the constraint that a steel wall would be driven to terminal velocity of approx. 1000m/s. 1-D Gurney theory [6] for finite-length cylinders, Eq. 1, provided a quick estimate that a steel cylinder of 0.40cm wall thickness would meet the velocity goal. This is a 33% increase in wall thickness and 47% reduction in wall velocity over previously analyzed cylinders of Ref. 1. This change of design warrants a new in-depth analysis to evaluate the loading conditions.

The Gurney Equation for a cylinder of finite length is:

$$V_G = \sqrt{2E}\left[\left(\frac{M}{C}+\frac{1}{2}\right)\left(1+\frac{R}{L}\right)\right]^{-1/2} \qquad (1)$$

Where V_G is the final velocity of the metal case (m/s), R is and L are cylinder radius and length, respectively. Charge mass, C, and metal mass, M, per unit length just must be of equivalent units. The Gurney constant, $\sqrt{2E}$, is 1700m/s. The 0.40cm wall thickness is maintained as a constraint on all cylinders of this effort. A radius to length (R/L) ratio of 1/16 was specified, giving total cylinder length of 20.2cm (8in). Total length was not necessarily the length of the region having controlled loading. Some of the systems used 5.08cm (2in) long sections of copper at each end of the „specimen" section in order to minimize end effects of rarefaction and reflected waves. The copper was easily identified and discarded from other fragment materials in recovery experiments. Fig. 1 shows the cross-sections of the cylinder and

ring configurations having copper end constraints. Some additional cylinders were made from a single material (i.e. no Cu end pieces) of 20.2cm length.

NUMERICAL ANALYSIS

The OTI-HULL code [5] was used to computationally explore and evaluate the cylinder designs. HULL employs an Euler/Lagrange interactive link with the explosive modeled in the Euler grid and the cylinder in the Lagrangian module. "Tracer" particles were placed in several locations through the wall thickness to ensure differences between the high pressure detonation interaction and the outer free-surface regions all reached similar loading conditions before the time of fracture.

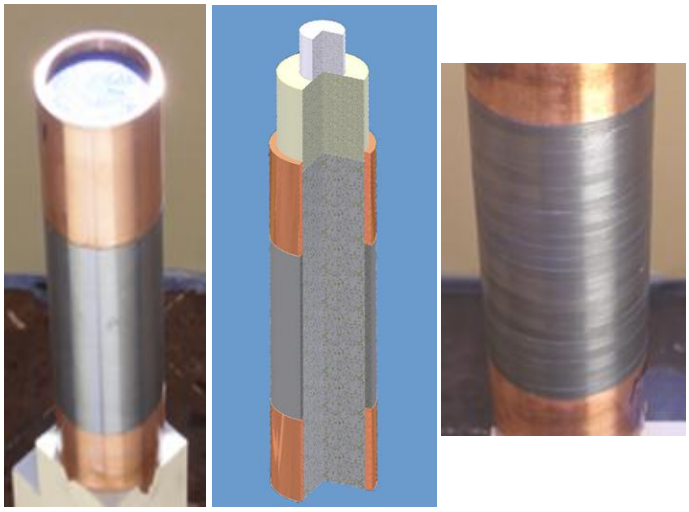

Figure 1. Cylinder of uniaxial stress (left 2) and plane strain stack of rings (right). Cu end sections provided clean boundary conditions for the central 'specimen' sections.

Stress triaxiality is the criteria used in determining the loading conditions. Triaxiality is defined as the ratio of the mean stress, $-\bar{\sigma}$, (or hydrostatic pressure, -*P*) to the vonMises stress, σ_M, as defined by Eq. (2).

$$\sum = \frac{-P}{\sigma_M} \qquad (2)$$

with vonMises stress being an equivalent stress defined by, $\sigma_M = \sqrt{\frac{3}{2}\sigma'_{ij}\sigma'_{ij}}$ (3) having σ'_{ij} as the stress deviator components. The plane strain establishes a condition of $\sum$ = 0.577 and uniaxial stress being $\sum$ = 0.33. Notice that for this effort a minus sign is introduced to give triaxiality as negative in compression and positive in tension. Also, note that this is a time and location dependent value that should converge to the appropriate condition as the detonation wave passes the cylinder, the transmitted shock reverberates within the wall thickness, and the cylinder expands to failure. Thus, two loading paths are achieved from a common cylindrical explosive configuration by just varying its length: a thin-walled, long cylinder under pure radial expansion for plane strain loading and a thin-walled ring with uniform radial expansion for establishing uniaxial stress loading. Investigations were also made on the minimum length required by a cylinder to still maintain plane strain conditions.

Numerical investigations were conducted on the cylinders and metal tube dimensions to ensure that triaxiality conditions were met. Variations investigated include:

1. Cylinder materials – Steel, Cu, Ta, W-alloy
2. Detonation scheme – endpoint, end plane, centerline
3. Cylinder Length – ring (0.4cm), 2.54cm, 10.1cm

All designs used an RDX-based blast explosive formulation. Its relatively low detonation pressure was desirable in maintaining lower axial and shear strains that adversely affect early-time triaxiality state response. An existing Jones-Wilkins-Lee (JWL) equation-of-state was used for the gas products [7].

PLANE STRAIN CYLINDER ANALYSIS

Our first discussion involves cylinders of ES-1. The ES-1 material, Ref. [8], was modeled using initial yield strength of 12.4kbar with 15.2kbar at 20% plastic strain. The initiation scheme, which does influence the loading conditions, was a plane-wave at one end of the 20.2cm long cylinder. A wall thickness of 0.40cm was used. Density plots of the steel cylinder are given in Fig. 2 as an initial orientation to calculations and discussion. The triaxiality response is seen in Fig. 3 for data taken at the mid-plane (10.1cm) and four radial positions through the wall thickness (r = 2.57, 2.68, 2.80, and 2.91cm). Unless otherwise stated, all data is reported from tracer points on the plane at mid-length on the cylinder. The response shows initial stress transients of the detonation and shock response, but that stress conditions converge to triaxiality condition of plane strain in time. Therefore, a key characteristic of this event is the time dependent evolution of plastic strain and does it correlate to triaxiality states before strain to failure conditions occur. The time evolved plastic strains for the radial monitor points are given in Fig. 4 along with a strain measured by simple reduction in case thickness or "thickness strain", ε_{tt} of Eq. 4,

$$\varepsilon_{tt} = -\ln\left(\frac{t_{final}}{t_{initial}}\right) \quad (4)$$

where $t_{initial}$ is the initial wall thickness and t_{final} is its thickness at a later time of interest. Thickness strain is a parameter that will compare directly to measurements of the experimentally recovered fragment thicknesses. The plane strain cylinders have an equivalent plastic strain (eps), $\bar{\varepsilon}$ relation to the thickness strain of,

$$\bar{\varepsilon} = \frac{2}{\sqrt{3}}\varepsilon_{tt} = 1.15\varepsilon_{tt} \quad (5)$$

with Eq. 5 defining that the net plane strain eps as 15% higher than the through thickness strain. The computed plastic strain values, Fig. 3, also account for the compression and tensile release strains from the passing detonation shock front. This loading history creates a nearly 10% to 20% initial strain, depending on location within the wall and cylinder material strength. It is assessed from Figs. 3 and 4 that the ES-1 cylinder should not fragment before 35us in order to meet plane strain conditions. These data will serve as key assessment points in the experiments and ultra-high speed photography of the fracturing cylinder.

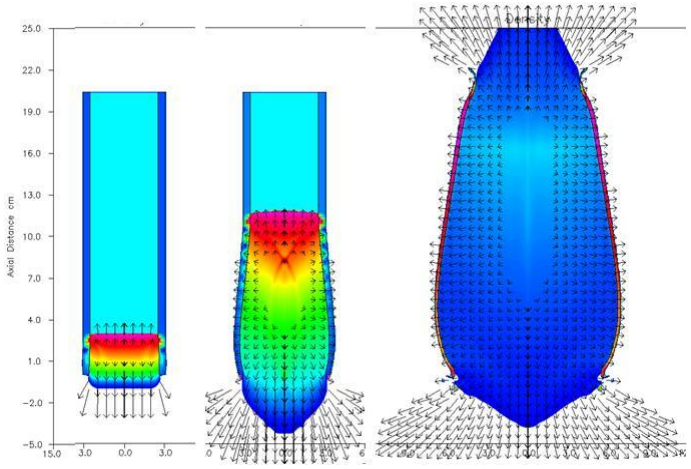

Figure 2. End-initiation of ES-1 cylinder at 5us (left), 20us (center), and 60us (right)

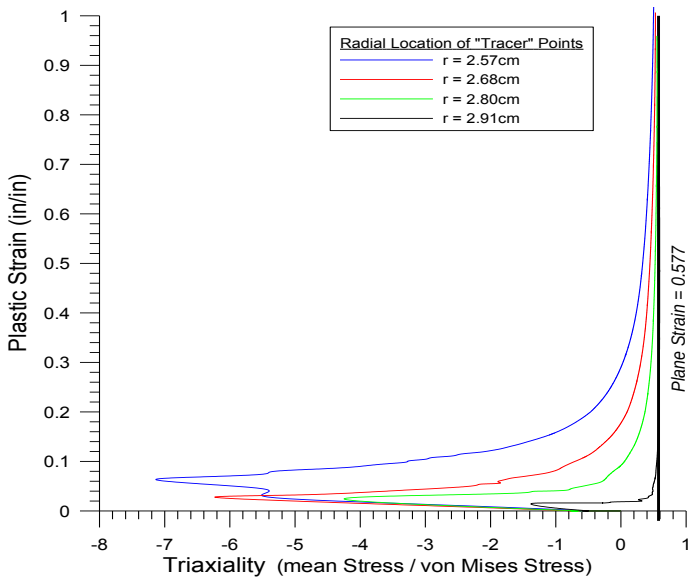

Figure 3. Triaxiality response through ES-1 cylinder wall at a mid-plane position (10.1cm from initiated end)

The effect of cylinder material, but more importantly material strength, is illustrated by comparing the triaxiality response of the steel cylinder (Fig. 3) with that of an entire cylinder of pure Cu (Fig. 6). The Cu has initial yield strength of 1.2kbar and work hardens to 4.5kbar at 30% strain. Both have wall thicknesses of 0.40cm. At this time, it is convenient to introduce the influence of the initiation scheme on the loading condition. The two initiation schemes for the pure Cu cylinders, shown in the density plot of Fig. 5, are an end-initiation plane-wave and the full centerline axis.

Comparison of the end initiated Cu in Fig. 6 with the end initiated ES-1 in Fig. 3 shows both materials eventually converge to ideal plane strain conditions of 0.577, but at greater plastic strain for the ES-1. The early, greater triaxiality of the Cu is simply that its effective stress is limited by the lower yield condition. This is especially true for data from the inner tracer locations affected by the axial strains from the detonation shock front. Load path and strain history effects for the Cu material give rise to greater disparity between the tracer locations and that of the through thickness strain, seen in Fig. 7.

Referring to Fig. 6, the centerline initiation scheme appears to show a reduction of the plastic strain (hence, time) to converge to plane strain conditions over that of the plane-wave end ignition However, upon closer inspection the responses become similar in value around 40% strain and it"s not until nearly 100% strain that values of the outer radii locations converge to plane-ε conditions. The centerline scheme was thought to offer improved, more direct radial expansion, but the analysis shows there is no such benefit. Additionally, the centerline scheme is easily achieved computationally, but it would not be so experimentally.

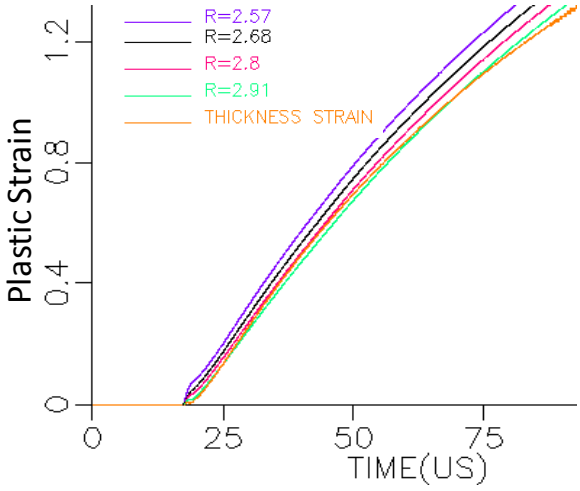

Figure 4. Time dependent plastic strain of ES-1 cylinder

CYLINDER LENGTH ANALYSIS

Further analysis was completed to examine plane strain conditions as a function of cylinder length. Steel cylinders of lengths 20.2cm, 10.1cm, 5.08cm, 2.54cm, and 0.40cm were analyzed with tracer data reported at the cylinder"s mid-length plane and four other locations equally and symmetrically located about this mid-plane. The cylinder wall had seven (7) elements through the Lagrangian wall and four tracer locations through the wall thickness. Each of the shorter cylinders (<20.2cm) were "sandwiched" between additional steel and Cu end-cylinders to maintain a total system length of 20.2cm; but, more importantly, controlled boundary conditions. The central ES-1 cylinder, „specimen", is a separately defined material from the surrounding ES-1 cylinders. The 25.4cm arrangement is shown in Fig. 8 to include the explosive booster train system. This initiation configuration approaches the plane-wave initiation scheme of earlier.

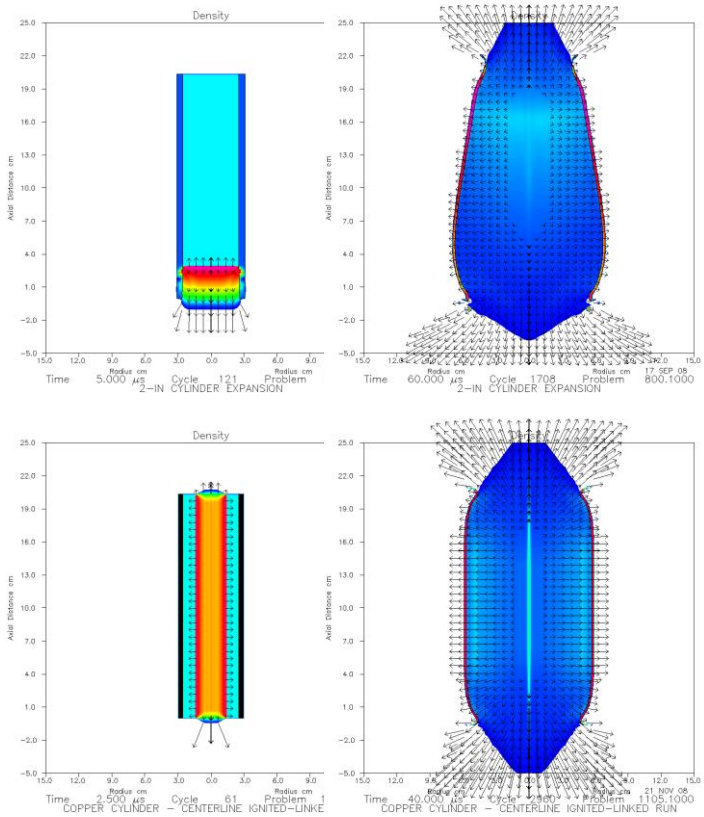

Figure 5. End-initiation at 5 and 60-us (top) and centerline initiation at 2.5 and 40-us (bottom) of Cu cylinders

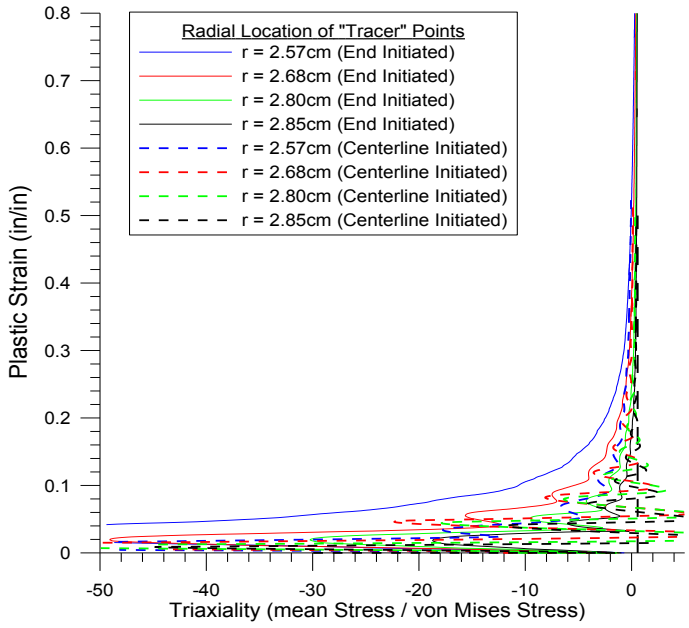

Figure 6. Cu cylinder responses with Plane-wave End and Centerline initiation schemes

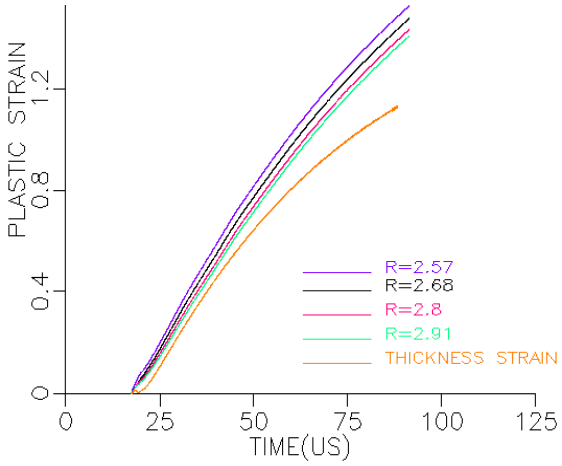

Figure 7. Plastic and thicknesss strain of plane-wave end initiation of Cu cylinder

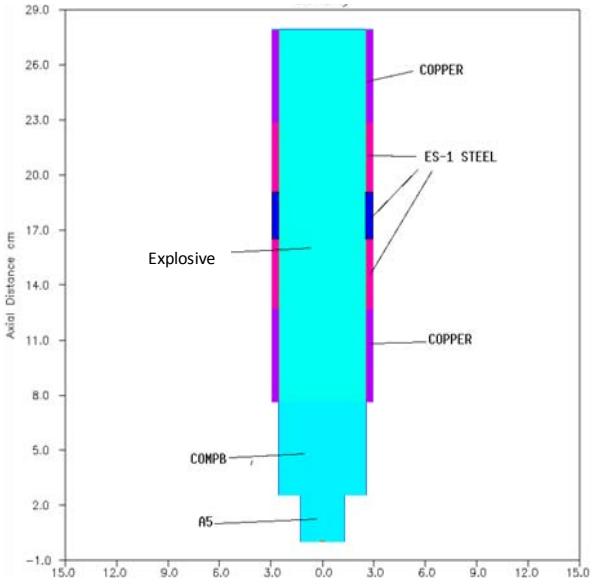

Figure 8. Arrangement for shorter cylinder specimen lengths

It was realized during the conduct of this cylinder length study, that the early time loading states were all very similar, regardless of cylinder length. The triaxiality condition varies with internal pressure and reaches their end-state values as the pressure decreases and the plastic strain increases. A criterion to distinguish the difference from the full cylinder, i.e. plane strain response, was established; a „critical strain" was defined to be the strain at which the triaxiality response departed from that of the full length cylinder. This is illustrated in Fig. 9 for the 2.54cm and 5.08cm long cylinders, both at the inner radial tracer point, r = 2.57cm. The critical strain is about 40% for the 2.54cm and 80% for the 5.08cm long ES-1 specimen. Approximate values here are acceptable because critical strain varies with radial tracer location. A table of all critical strains for the various cylinder lengths is given in Table 1, below. From this data and the knowing the approximate strain to failure of ES-1, it is reasoned that a cylinder of only 5.08cm long is required to achieve plane strain response. Recall, that the strain values of the tracer points are greater than that of through thickness strains and failure strains measured accordingly. This study would be useful for efforts desiring limited material, limited explosive quantity or other reason that full length (20.2cm) specimens were not available.

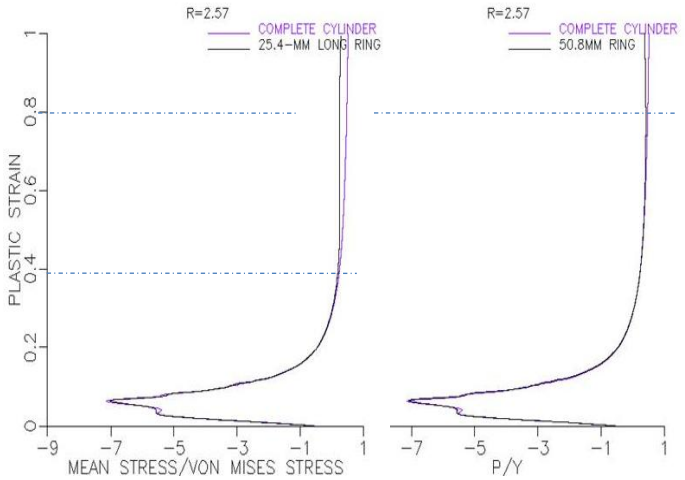

Figure 9. Example of the critical strain defined for cylinder lengths of 2.54cm and 5.08cm

Table 1. Critical strain values for various cylinder lengths

Cylinder Length (cm)	$\varepsilon_{critical}$ % r_1=2.57cm	$\varepsilon_{critical}$ % r_2=2.68cm	$\varepsilon_{critical}$ % r_3=2.80cm	$\varepsilon_{critical}$ % r_4=2.91cm
0.40	35	30	20	5
2.54	40	30	30	20
5.08	80	70	65	60

UNIAXIAL STRESS RINGS ANALYSIS

The shortest length cylinder, 0.40cm long, provides the specimen design of the uniaxial stress conditions. The „rings" of 0.40cm length and 0.40cm wall thickness were analyzed for the ES-1 and the Aero224 tungsten alloy. Availability of the W-alloy in limited lengths made it best suitable for analysis in the ring configuration.

The cylinder system for uniaxial stress was designed similar as previous, with the pre- and post- sections of copper. The loading history from the tracer points are given in Fig. 10 along with a density map of the simulation at 30us time showing the small ring at the cylinder"s mid-length. Data available for Aero224 under dynamic tension lists the failure strain at less than 5%. So, the response of Fig. 10 means that rings of this brittle material will not have converged to uniaxial stress conditions. Simulations conducted for rings of ES-1, reported in the previous section and Table 1, gave a range of critical strains to have acceptable uniaxial stress approximations before failure. The convergence is good enough to proceed with experiments and obtain in situ measure of the thickness strain.

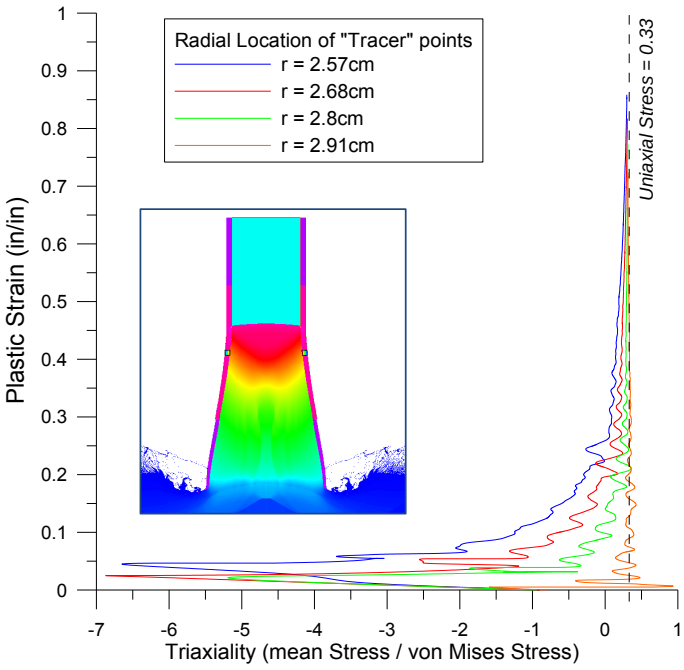

Figure 10. Triaxiality response of a 0.40cm long ring of Aero224, W-alloy.

CYLINDER EXPERIMENT

A limited number of experiments were conducted in parallel with the computational analysis. The two types of experiments provide a fairly complete characterization of the cylinder fragmentation data. The first type is an open air fragmentation of the plane strain cylinders using ultra-high speed photography and velocity diagnostics. Expansion velocity, strain rate, cylinder rupture and fragmentation characteristics are obtained from the open air experiment. The second experiment type is a fragment recovery method. Cylinders and the ring systems are set inside a dense foam structure of approximately 100cm diam. by 100cm tall that itself is placed within a 1000-gal water tank. The cylinder or rings are allowed to expand and fracture within the air void of the foam surround but then decelerate through the foam and slowed for recovery in the water. This method [Refs. 1, 4] has typical recovery rates of ~95%. This method preserves the *in situ* state of the fragments for extracting strain to failure measures, fragment size and mass distributions, as well as metallographic investigations of the fractured materials. Water recoveries were made for the ES-1 cylinders and Aero224 rings and are discussed in more detail in Refs. [2,10].

DISCUSSION OF EXPERIMENT AND SIMULATION DATA

The most interesting and relevant of the experiments was the cylinder (plane strain) test of ES-1. A cylinder of 20.2cm length of ES-1 was explosively filled and had an initiation train consisting: an exploding bridge wire detonator, boosted by a 2.54cm diam. by 2.54cm long cylinder of Composition A-5 and then a 5.08cm diam. by 5.08cm long cylinder of Composition B. A Cordin 132a rotating mirror, ultra-high speed framing camera was used to capture the cylinder‟s expansion and plastic deformation. A three channel photonic Doppler velocimetry (PDV) [7] system provided ns-time base resolution of wall-velocity. A pre-test photograph of the ES-1 cylinder and the locations of the PDV probes are shown in Fig. 11.

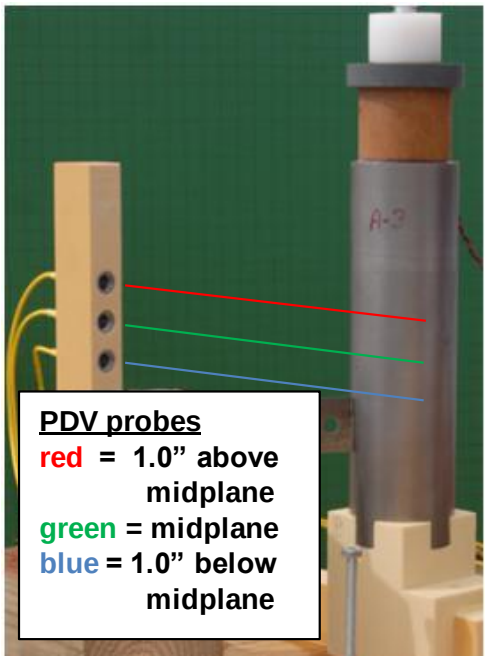

Figure 11. ES-1 plane strain cylinder with PDV probes

Select images from a 45 frame sequence taken at 1.0us/frame for the ES-1 cylinder are seen in Fig. 12. They are invaluable to linking the physical fragmentation processes and cylinder response to that of the code simulation data. These images, with their time-base synchronized to PDV probe data of Fig. 13, help isolate the time of fracture of the cylinder which can then be related back to the plastic strain-vs-time traces of the simulations. The code simulations must have approx. 14-us (+/- 2us) added to them (function time of the initiation train leading to the cylinder) for direct comparisons. The images *qualitatively* show fracturing and fragmentation occurring at the mid-length (green line of Fig. 12) at around 35us. The PDV data helps bracket the timeline of fragmentation because the wall at this location does not begin expanding until 31.35us. Thus, the time-adjusted response of Fig. 4 indicates a plastic strain of 60% for thickness strain and up to 75% for the inner r = 2.57cm location. We now refer back to Fig. 3 to see that these high plastic strain values give increased confidence that the plane strain approximation is being met before fracture.

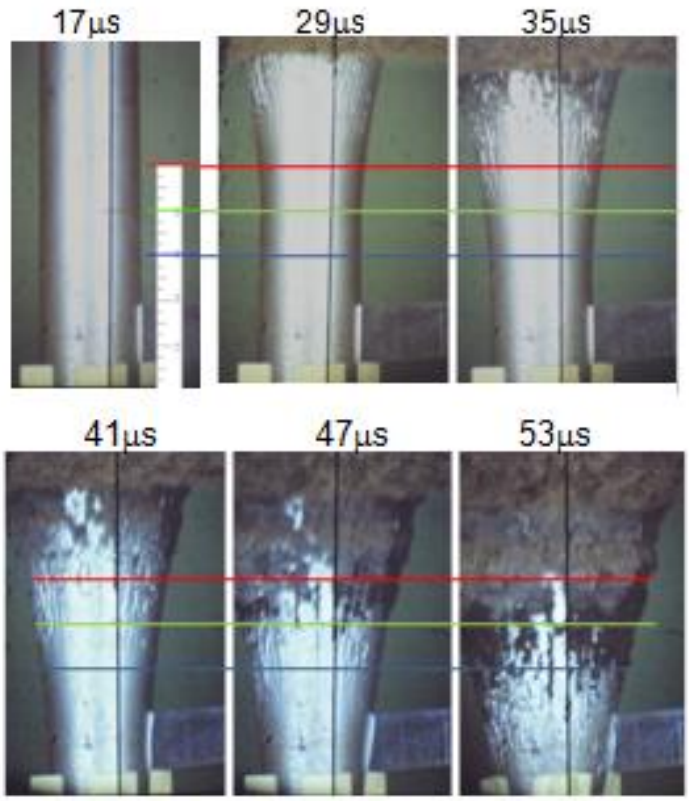

Figure 12. Plane strain cylinder fracture of ES-1.

(The colored lines denote the locations plane of PDV data reported in Figs. 11&13.

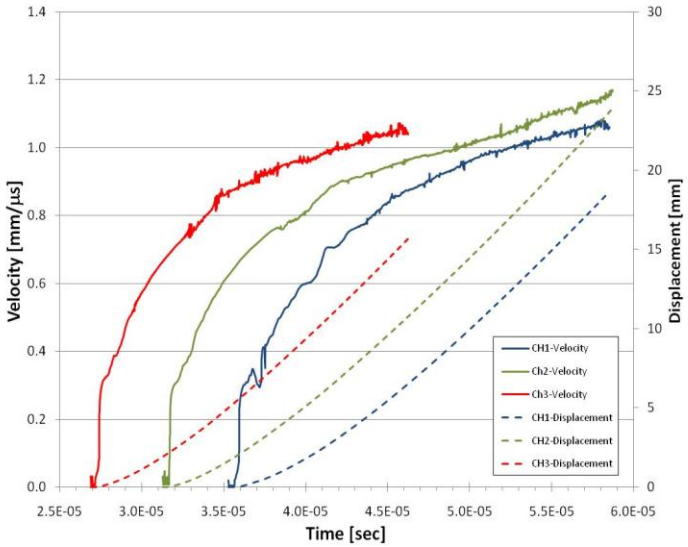

Figure 13. PDV probe responses at locations 7.62cm, 10.16cm, and 12.70cm from the cylinder end (color-coded to lines in Figs. 11&12).

CONCLUSION

A series of computations on the explosively loaded cylinder systems has been presented to help extend its utility as a controlled loading mechanism in high rate material studies. The goal of meeting plane strain or uniaxial stress conditions varies with material strength, initiation scheme, and cylinder length. Here, a constrained wall thickness of 0.40cm and terminal wall velocity of 1000m/s was used to evaluate candidate systems for which to proceed with experiments. Additionally, specific materials selected for study, the ES-1 steel and a tungsten-alloy Aero224, were analyzed for their ability to attain the necessary triaxiality conditions prescribed by either plane strain or uniaxial stress before fracture occurred. This has resulted in partial success. Correlations between experiment and simulation were tremendously successful in establishing the plastic strain versus time versus triaxiality state. The PDV and ultra-high speed photography data proved to be an invaluable linkage on future studies. However, the analysis on the ring system of Aero224 was not as promising. The strain to failure for this rather brittle material is too low to enable plane strain conditions to develop before fracture occurs.

Future efforts will continue on these cylinder systems with experiments of water recovery for ES-1 ring and full cylinder systems already underway. The physical recovery of the fragments will provide the necessary measures of thickness strains leading to verification of equivalent plastic strains and further corroboration with simulation results.

Not addressed within this paper is, perhaps, the harder portion of the effort. This is the collection and statistical distribution of the failure strains and fragment sizes that feed into the compensated fracture models within the continuum design codes. Never the less, this effort will continue with such goals to improve capabilities and design tools of fragmenting items.

ACKNOWLEDGMENTS

The authors must give credit and appreciation to D.M. Goto and T.J. Orzechowski, and their colleagues at Lawrence Livermore National Laboratory for their substantial contribution of information, drawings and advice. Acknowledgment is made to Dr. Eric Welle and 1Lt. Timothy Ager of AFRL/RWMF for support and guidance on the PDV measurements. Lastly, the technicians at the Advanced Warheads Experimentation Facility, for continued expertise in the conduct and support of experiments.

REFERENCES

1. Goto DM et al, Investigation of the fracture and fragmentation of explosively driven rings and cylinders. *Intl J. Impact Eng*. 2008; **35**(12): 1547-1556.

2. Weiderhold J, DE Lambert, MV Hopson. Experimental design and data collection for dynamic fragmentation experiments. *Proc. 2010 PVP Conf.*, Bellevue, WA. Jul 2010.

3. Johnson GR, Cook WH. Fracture characteristics of three metals subjected to various strains, strain rates, temperatures and pressures*. Engng. Fract. Mech.* 1985; **21**(1): 31-48.

4. Hopson MV, CM Scott, R Patel. Computational comparisons of homogeneous and statistical descriptions of AerMet100 steel subjected to high strain rate loading. *Proc. 11th Hypervelocity Impact Symp*. 2010; in print. Freiburg, GE.

5. Matuska DA, JJ Osborn, EW Piburn. *The HULL user's manual*, Orlando Technology, Inc., Shalimar, FL 1991.

6. Gurney RW. The initial velocity of fragments from bombs, shells, and grenades. *Army Ballistic Research Laboratory Report* No. 405 1943.

7. Lee EL, HC Hornig, JW Kury. Adiabatic expansion of high explosive detonation products. *Lawrence Radiation Laboratory Report* No. UCRL-50422 May 1968.

8. Dilmore M, Eglin Steel – A low alloy high strength composition. US Patent 7,537,727B2. 26 May 2009.

9. Strand OT, DR Goosman, C Martinez, TL Whitworth, WW Khulow. Compact system for high-speed velocimetry using heterodyne techniques*. Rev. of Sci. Inst*. 2006; **77**:08310.

10. Hopson MV, DE Lambert, J Weiderhold. Computational comparisons of homogeneous and statistical descriptions of steel subjected to explosive loading. to be published in *Proc. 2010 PVP Conf.*, Bellevue, WA. Jul 2010.

CHAPTER 2

Proceedings of the 2009 Pressure Vessels and Piping Conference

PVP-2010

July 18-22, 2010, Bellevue, Washington, USA

PVP-2010-25163

Paper PVP2010-25051

Dynamic Fragmentation Experiments Under Plane Strain and Uniaxial Stress Conditions

1st Lt Joseph Weiderhold
Air Force Research Laboratory
Munitions Directorate
Eglin Air Force Base, FL, USA

David E. Lambert
Air Force Research Laboratory
Munitions Directorate
Eglin Air Force Base, FL, USA

Michael Hopson
Naval Surface Warfare Center
Dahlgren Division
Dahlgren, VA, USA

ABSTRACT

Experiments have been conducted to investigate the fracture and fragmentation characteristics of a liquid phased sintered (LPS) tungsten and high strength steel alloys. Metal cylinders, each of which was 20.32 cm tall and 5.08 cm inner/5.88 cm outer diameter, were explosively driven to failure. Two complimentary types of experiments were conducted in this series to determine input parameters for a related continuum mechanics based modeling effort. Open air experiments utilized ultra-high speed framing photography and a photonic Doppler velocimetry system (PDV). The information from these experiments provided a case wall velocity, relative time of breakup and strain-rate during the stress loading timeframe. Complimentary experiments were conducted in a water tank to perform a soft recovery of the fragments. The fragments were subsequently cleaned, massed, and characterized according to their mass and failure strain distributions. Various methods of analyzing the data (Mott & Weibull distributions) are discussed along with the calibration of the continuum damage model parameters. Results of the failure strain analysis, fragment distribution, and damage model are then supplied for use in subsequent modeling and application designs.

Further details of the modeling and simulation approach are outlined in a complimentary set of two papers presented by Lambert [1] and Hopson [2].

INTRODUCTION

The explosively loaded cylinder is perhaps the most commonly used configuration of all explosive-related studies. From an engineering perspective, it provides a representative geometry of a large class of applications. Air delivered weapons, which are loosely classified based on their mass-to-charge (M/C) ratios, fall into several categories. Armor piercing, semi-armor-piercing, general purpose, and modern penetrating weapons all vary the characteristic M/C ratio to achieve different results. .

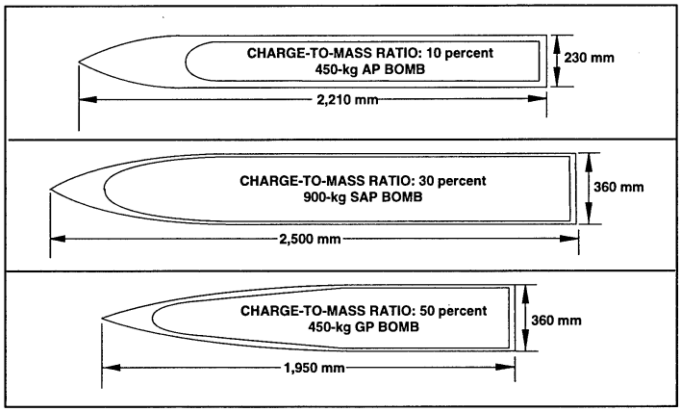

Figure 1. Notional depictions of armor piercing (AP), semi-armor piercing (SAP), and general purpose (GP) bombs [3]

The fracture and fragmentation of the case after the weapon detonates are increasingly important as lethality predictions guide engagement scenarios.

Typical metrics for measuring the performance of fragmenting weapons are obtained from arena tests. These experiments, while indicative of the late-time behavior and terminal effects of the fragment fly out, provide little information about the case failure and do not allow a weapon designer to actively predict or design performance characteristics without extensive testing. For this reason, capturing relevant early-time performance is vital to validating computational methods designed to understand and physically model the event.

The seminal work of N.F. Mott [4], G.I. Taylor [5], D.E. Grady [6,7], T.J. Vogler [8], and many others established a solid foundation from which to obtain engineering design parameters for fragment sizes, size distributions, fracture strains, and dynamic strength measures. The more recent work of Goto, et al [9] expands on this collection of research efforts to further establish the explosively driven cylinder as a benchmark for relevant engineering properties data.

In the present experiments, two different arrangements were selected to produce a predictable stress-loading state. Data used from these experiments is integrally linked with the calibration of engineering fracture models that determine failure based on a scalar damage parameter. Implicit in the design of many fracture codes is the assumption that microstructure heterogeneity is not captured in equation constants, but must instead be compensated for using statistical methods.

CYLINDER MATERIAL

There were two materials of interest in this cursory set of experiments: a new high-strength steel, Eglin Steel (ES-1), and a tungsten alloy, Aero-224. The steel was developed jointly by AFRL/RW and Ellwood National Forge Company as an ultra-high strength, high toughness steel that is cost effective to produce. Typical dynamic response as experimentally shown by Torres et. al [10] is shown in Fig. 2. This information is derived from modified small-caliber Taylor anvil tests.

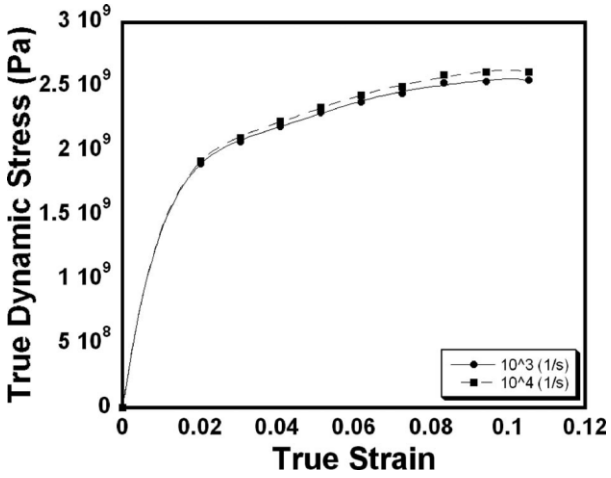

Figure 2. Dynamic response of ES-1 steel at varying strain rates (courtesy K.L. Torres [10])

The steel was rough machined, heated in a vacuum furnace at 1850 °F for one hour followed by an oil quench. The steel was then tempered in an air furnace at 400 °F for a total of four hours followed by air cooling. This heat treatment process was determined to give an acceptable balance of impact toughness, strength, and ductility.

Aero-224 is a high-strength, high-ductility alloy comprised of tungsten particles in a composite nickel/cobalt matrix. Among tungsten heavy alloys, Aerojet Ordnance Tennessee (AOT) has developed a proprietary processing method that produces an alloy capable of bearing the heavy transverse loading normally experienced with both anti-armor and hard-target defeat [10]. Material property data for this alloy varies widely due to the different methods of cold working (swaging) that exist for the material. Since the material is typically used in small diameter (< 5 cm) applications for kinetic energy rod penetrators, little performance data exists for swaged material at larger scales. In a related research and development effort conducted between AOT & the Advanced Warhead Experimentation Facility, a 7.62 cm diameter bar of Aero-224 material was cold worked at the AOT facility in Jonesborough, TN, USA. This effort was unsuccessful and the swaged bar experienced only approximately 4.2% reduction in area. The present research considers only the behavior of the unworked (as cast) Aero 224 alloy.

In generating material behavior data for a Johnson-Cook strength model [12], the material was subjected to a variety of quasi-static and dynamic tension and compression events. High strain-rate testing was accomplished with a 5/8” (1.588 cm) diameter split Hopkinson pressure bar. The results of these experiments are shown in Fig. 3.

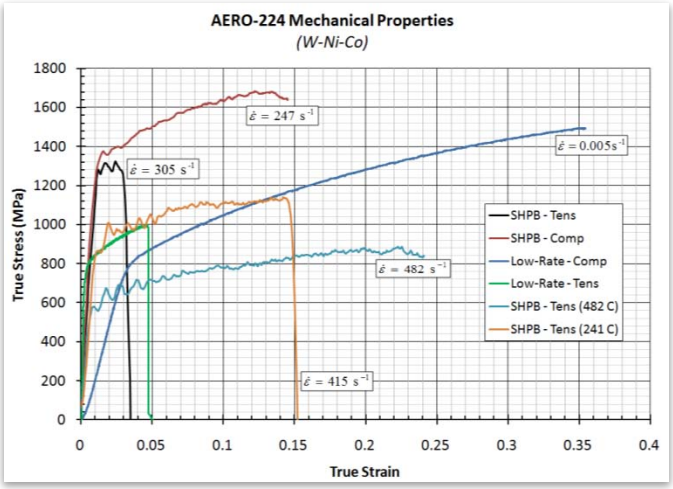

Figure 3. Mechanical characterization of Aero 224 alloy accomplished at the AWEF facility (courtesy Philip Flater, AFRL)

As indicated in Fig. 3, the alloy did not demonstrate significant ductility in tension experiments. Close examination of the fracture surfaces on the sample corroborate the brittle failure witnessed during testing.

The materials were driven by an explosive having roughly 25% RDX, 33% aluminum and 30% ammonium perchlorate with the remaining constituents being binder and plasticizer materials. This formulation is typically geared for a blast event, but the lower detonation pressures (relative to high RDX percent compositions) provides reduced shock loading and more gradual acceleration. A Jones-Wilkins-Lee [13] product equation of state was previously calibrated at a relevant 2-inch cylinder size for design and modeling of these experiments.

CYLINDER DESIGN

An axisymmetric cylindrical geometry is used with explosive core based on a 5.08cm (2.0 inch) casting diameter. The metallic tube thickness was chosen using the constraint that a steel wall would be driven to terminal velocity of approximately 1300 m/s. 1-D Gurney theory [14] is used for the initial broad look at the design space of cylinder materials and thicknesses. Velocity predictions for a 0.40 cm wall thickness, finite length cylinder are determined by Eq. 1, with values for various other metals tubes given in Table 1.

$$V_G = \sqrt{\frac{2E}{\left[\frac{M}{C}+\frac{1}{2}\right]\left[1+\frac{R}{L}\right]}} \qquad (1)$$

where V_G is the final velocity of the metal case, and R and L are the cylinder‟s radius and length, respectively. The Gurney constant ($\sqrt{2E}$) used for this explosive was approximately 1700m/s.

Table 1. Gurney Velocity for Various Metals of 0.40cm Wall-Thickness

Cylinder Material	density	Charge (g)	Metal (g)	M/C	V (m/s)
Aluminum	2.7	757.81	377.81	0.499	1585
Zirconium	6.51	757.81	910.95	1.202	1214
Steel	7.8	757.81	1091.46	1.440	1137
Copper	8.94	757.81	1250.98	1.651	1080
Tantalum	16.6	757.81	2322.86	3.065	839
Aero 224 Tungsten	17.4	757.81	2434.80	3.213	822

A thin walled cylinder represents a plane-strain condition when subjected to a purely radial expansion and having a stress triaxiality of 0.577. (Stress triaxiality is defined as the ratio of the mean stress to the von Mises stress, $\sum = -P/\sigma_M$.) A thin walled ring, on the other hand, expanding uniformly in the radial direction corresponds to a state of uniaxial stress with triaxiality of $\Sigma = 0.33$. Hence, two loading paths can now be achieved from a common cylindrical explosive driver system by just varying the cylinder length. However, numerical investigation is required to ensure that triaxiality conditions are met in the cylinder walls during the event time from explosive launch to severe plastic deformation and incipient failure.

The design of the plane strain cylinder (ES-1 case material) comprised of a two stage booster (RP-1 initiator to Comp A-5 to Comp B) that established a planar detonation front transfer to the main cylinder charge. The explosive charge was 20.32 cm in length. The steel cylinder overlapped the Comp B boosted by approximately 0.64 cm in in order to ensure a perfectly concentric mate between the booster and main charge. A depiction of this test configuration is shown in Fig. 4.

Figure 4. Eglin steel test article with booster assembly and mating fixtures shown

Uniaxial stress experiments for the Aero 224 tungsten alloy utilized a configuration that allowed for multiple ring experiments to be simultaneously conducted. While the booster train and main charge configurations were identical between these experiments and the plane strain condition experiments, the dimensions of the case material were changed significantly. A 5.715 cm long run length using copper confinement (0.40 cm wall thickness) helped minimize end-effects of rarefactions and establish quasi-steady state detonation conditions. That was followed by a 10.16 cm long cylinder of the material being studied and then a final 5.08 cm run length, again using copper, to mitigate end-effects and rarefaction waves moving back into the expanding “test section” too early. This configuration also allowed for a 0.64 cm overlap between the

copper sleeves and the Comp B booster. A total of 25 rings, each 0.4 cm in both thickness and height (as shown in Fig. 5), were loaded between the two copper sleeves. Maintaining the same dimensions for the rings in both length and height allowed for the assumption that deformation and strain in these directions could be measured and calculated interchangeably upon recovery of the fragments.

The cylinder and ring dimensions were not arbitrarily selected. The HULL code, a continuum-mechanics based hydrocode, was used to analyze the stress triaxiality condition of the cylinder and ring sections over the loading period. The simulations presented in reference [1] provide a verification that these dimensions, for the particular metal and explosive drive, result in the appropriate uniaxial stress or plane strain condition as the cylinder (or ring) is driven to failure.

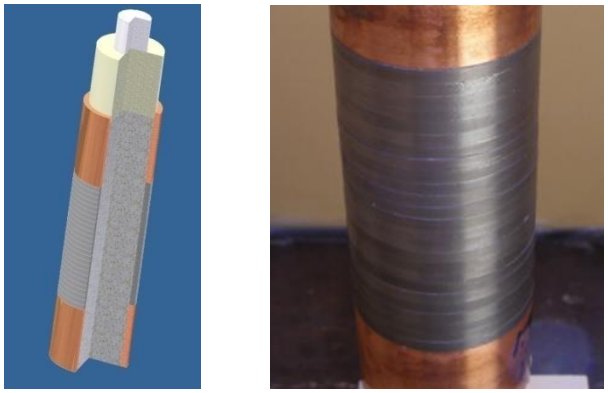

Figure 5. Aero 224 test article CAD drawing (left) showing rings, copper sleeves, and explosive assembly; actual test item (right) positioned inside catch tank

EXPERIMENT DESIGNS

The primary objective of the experiments was to quantify strain-to-failure, fragment mass and fragment size distributions under dynamic loading. Data of cylinder expansion to fracture, wall velocity, and recovery of the physical fragments dictated experimental designs. Two different types of experiments were used. The first was real-time capture of the cylinder expansion and plastic deformation to failure using an ultra-high speed framing camera. The Cordin 330 is a continuous access, rotating mirror camera that provides 80 images at speeds up to 2×10^6 frame/sec. High intensity illumination is required at those speeds and it was achieved using argon flash bombs. Illumination time for the flash bombs is determined based on a curve fit empirically determined by Davis et al. [15]:

$$x = 697(1 - e^{-0.013t}) \qquad (2)$$

where x is distance from the originating explosive that the shockwave has traveled through the argon, in mm, and t is the time elapsed since detonation.

Experiments of the plane strain cylinders were conducted with the Cordin camera and argon bomb setup. The uniaxial stress cylinders (i.e. stack of rings) were not used in the framing camera experiments because the air gaps between rings would allow for the high pressure gas products to release early and rapidly enough to obscure the view before failure.

A photon Doppler velocimetry (PDV) system provided case wall expansion velocity of the plane strain cylinders. This data is used to corroborate modeling and simulation analysis of the loading conditions. Wall velocity influences the stress triaxiality value as a function of time and, hence, plastic strain. A four channel PDV system monitored the cylinder at separate locations over an expansion range of up to 40 mm. Probes captured data at 101.6 mm (as measured from the bottom of the cylinder) and at points 25.4 mm above and below this point. The probes were fully fixed in bracket arm attached to a cradle for the cylinder. Both the cradle and bracket arm were manufactured from dense (20 lb /ft^3) and rigid foam. Optical characteristics of the probes used dictated a 250 mm standoff from the item. This standoff distance was selected based on the depth of focus afforded, previous success in testing at LLNL and LANL [16], commercial availability, and the presence of additional diagnostics (framing camera). Other similar tests were conducted with larger diameter probes at a shorter 100 mm standoff; results were generally comparable.

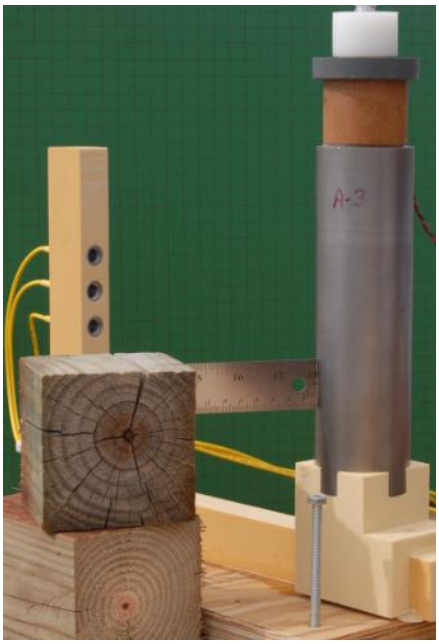

Figure 6. Eglin steel cylinder in an open-air configuration with PDV probe, bracket arm, and cradle

The second type of experiment was that of soft-recovery. Both the uniaxial stress and plane strain cylinder configurations used this method of safely decelerating and capturing the fragments from detonation. No camera or PDV probes were present in this configuration. Reliable mirror arrangements and probe bracketing would have interfered with the natural fragmentation process and a decision was made not to use these diagnostics in this configuration. Note that Fig. 7, which depicts the recovery apparatus, includes a

representation of a PDV bracket arm. This feature was not present in the final configuration.

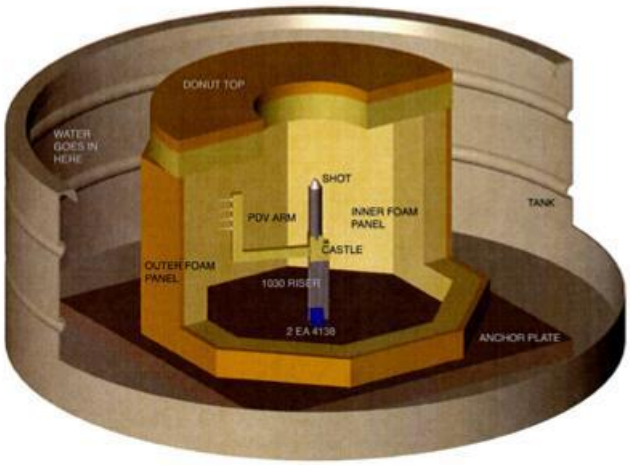

Figure 7. Fragment recovery apparatus (courtesy Dana Goto, LLNL)

The fragment capture apparatus consisted of a heavy foam octagon surrounding the cylinder resting on a stand. Silicone caulk was used to seal the foam and affix it to a 1.22 m x 1.22 m x 7.62 cm piece of mild steel. This thickness of steel was chosen to avoid having the foam octagon float due to the buoyant force created by the displaced water, as outlined in Eq. 3.

$$m_{steel} = \rho(2(1+\sqrt{2}))ah \qquad (3)$$

where m_{steel} is the minimum mass of steel necessary to avoid floatation, ρ is the density of water, *a* is the side length of the octagon, and *h* is the height of the octagon. This assembly rested inside of a white water tank which was highly effective at absorbing the blast from the event. However, the skin of the tank was punctured by one tungsten fragment. Typical response of the tank (captured with a Phantom v.12 camera) is shown in Fig. 8.

Figure 8. Water catch tank at full equatorial expansion as detonation products and foam are ejected

Even with the significant stresses imparted on the tank, it performed reasonably well in retaining all fragments.

RESULTS AND DISCUSSION

Typical recovery rates for the cylinders were on the order of 85-97%. The 25 rings shot as part of the uniaxial stress state Aero 224 experiment had an initial mass of 1.211 kg; a total of 1.184 kg of fragments were recovered. This 97.8% recovery rate was likely due to the tenacity of range technicians in ensuring every piece of recovered foam was thoroughly screened to ensure no fragments were present before the foam was discarded. A variety of magnets were used to help obtain smaller steel fragments and separate them from the mild steel base of the catch tank assembly. The magnets were not useful in the recovery of tungsten fragments. Fortunately the highly uniform distribution of the recovered tungsten fragments limited the quantity that was too small to recover. Recovered tungsten fragments had a mean mass of 1.05 g and a standard deviation of 0.39 g. The smallest fragment recovered was on the order of 0.17 g. On the other hand, naturally fragmenting steel cases produced fragments with a mean mass of 2.46 g and a much wider standard deviation of 2.32 g. The largest strip of steel fragment recovered was 12.33 g. Naturally fragmenting steel cases also produced many fragments smaller than 0.01 g. These fragments were separated and massed separately since individual measurements would have been outside of acceptable tolerances.

Strain measurements were readily accomplished for the tungsten fragments. A representative fragment (as viewed under a stereo light microscope) is shown in Fig. 9.

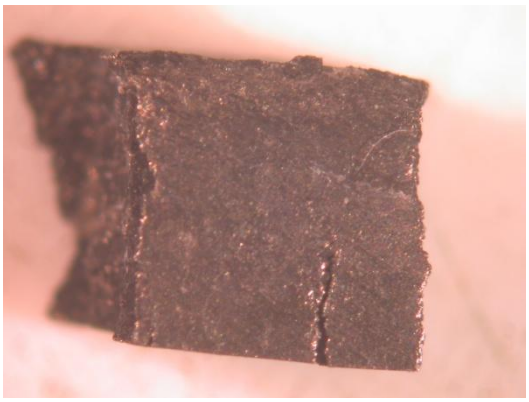

Figure 9. A typical recovered fragment of Aero 224 tungsten alloy viewed under a light microscope

These fragments had a height and through-thicknesss dimension of 4 mm before the detonation event. Upon recovery, through thickness and height dimensions were indistinguishable. Since the fragments failed in a uniaxial stress condition, failure elongation in either direction can be considered statistically identical. A total of 1,125 fragments were recovered and measurements were recorded. Logarithmic strain is defined as

$$\varepsilon = -ln\left(\frac{t_f}{t_i}\right) \qquad (4)$$

where t_f is the final thickness of a fragment and t_i is the ring"s initial height or thickness of 4 mm. Assuming a time-varying but geometrically uniform and symmetrical expansion of the ring occurs in uniaxial stress, the equivalent plastic strain (eps) at failure is defined as

$$\bar{\varepsilon} = \frac{2}{\sqrt{3}}\sqrt{({\varepsilon_t}^2 + {\varepsilon_h}^2 + \varepsilon_t \cdot \varepsilon_h)} \qquad (5)$$

where $\bar{\varepsilon}$ is the plane strain eps based on final deformation measurements of thickness and height logarithmic strains (ε_t & ε_h respectively) described earlier. Under the assumption that thickness and height logarithmic strain is statistically identical, Eq. 5 reduces to

$$\bar{\varepsilon} = 2 \cdot \varepsilon_x \qquad (6)$$

where ε_x is the logarithmic strain determined from measurement in either the thickness or height direction.

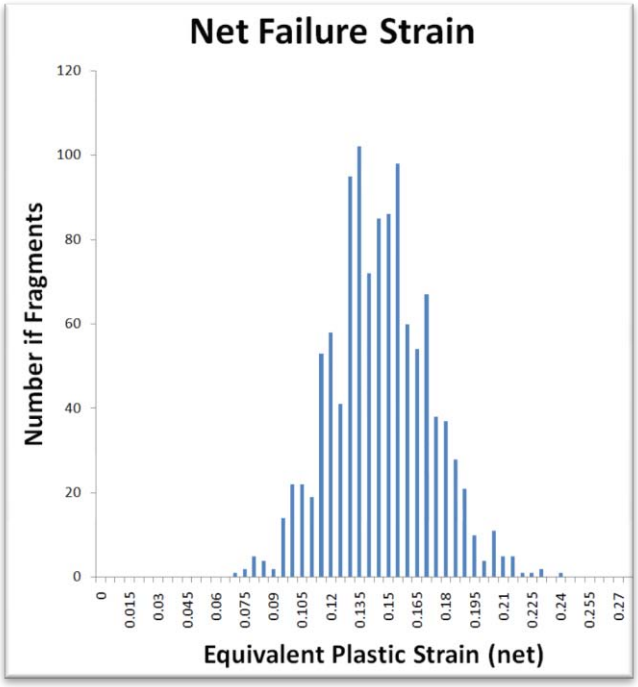

Figure 10. Failure strain distribution for Aero 224 rings

The distribution in Fig. 10 is centered around $\bar{\varepsilon} = 0.144$, which corresponds to a mean thickness/height measurement of 3.73 mm. Very little necking was observed in the recovered fragments, which corresponds with the low failure strain values recorded. Fig. 11 depicts a subset of the fragments and shows the nearly uniform size distribution.

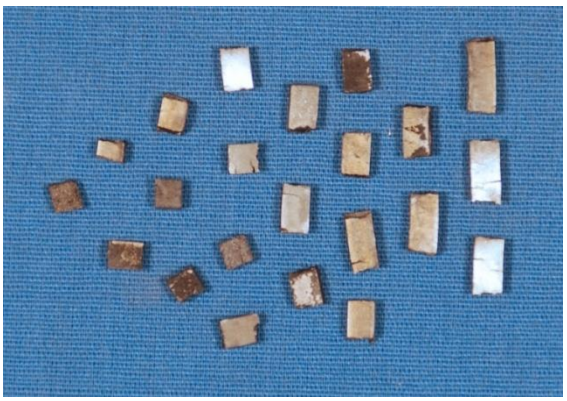

Figure 11. Subset of Aero 224 fragments from uniaxial stress ring configuration experiment

Measurements for the steel cylinder and rings were much more complicated and were ultimately not applied in this study. As is typically observed in the failure of naturally fragmenting steel cases, fracture surfaces were oriented at approximately 45° to the original inside and outside surfaces of the cylinder. Many of the rings exhibited similar fracture surfaces, as indicated in Figure 12.

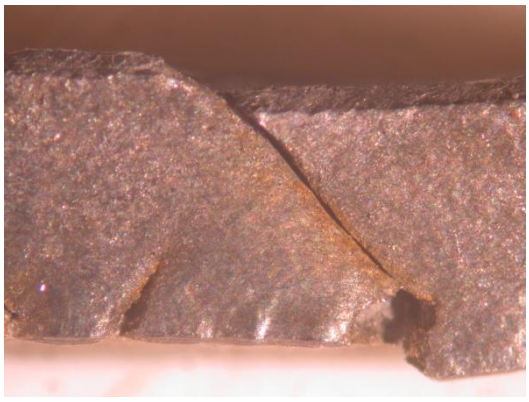

Figure 12. Fracture surface of recovered ES-1 ring

In many instances, this parallelogram shape (as viewed along the longitudinal axis of the cylinder) made for measurements that were inaccurate or not repeatable. A Mitutoyo™ digital micrometer was used for measurements. As an example, a single fragment that was measured in five locations and a range of observed thickness values from 3.45mm to 3.76 mm was observed. These measurements result in ε_t values that range from 0.062 to 0.148. This significant spread is influenced by human measurement bias (i.e. a tendency to measure the most readily accessible portion of a fragment, or only those that appear capable of being measured) along with surface features that allow a point micrometer to enter a crack and record a smaller thickness value than is physically relevant. Fragments from the ES-1 steel cylinder experiment varied much more in size and are shown in Fig. 13.

Figure 13. A portion of the fragments recovered from the ES-1 plane strain condition experiment

For these reasons, the fidelity of data obtained from steel cylinder strain measurements was deemed inappropriate for inclusion in the present model calibration studies.

Optical records of the event provide insight into the failure process but cannot be relied upon for successful measurement of failure strain values as a function of time. Physical limitations of the optical path from the Cordin 330 camera to the cylinder due to safety concerns limit the spatial resolution of returned images to approximately 0.5 mm. Additionally, only surface damage is visible and typically the cylinder has exceeded its mean failure strain at the point at which damage can be visualized. Instead, optical records are used to bracket the time of failure when interpreting PDV records.

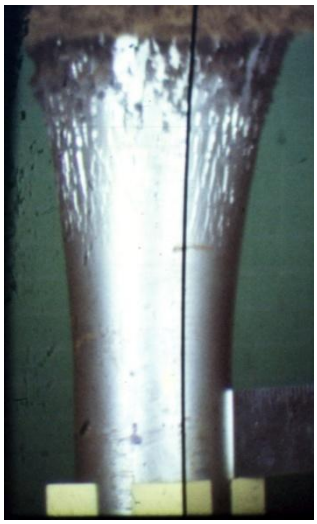

Figure 14. Optical image of expanding ES-1 steel cylinder

Photonic Doppler velocimetry records provided much more significant insight into the expansion event. High frequency DC-blocking band pass filters were used on all channels to reduce data drifting. This affected the resolution settings of the oscilloscope used to capture the data and in turn improved the signal-to-noise ratio of the returned light. This method proved to be very effective in achieving good temporal resolution. Additionally, a test shot was conducted with a single PDV probe aimed directly at the shocked argon bomb assembly. The probe returned only noise measurements and confirmed that there was not any IR radiation emitted by the light (~1550 nm for PDV) that might affect the cylinder wall return signal.

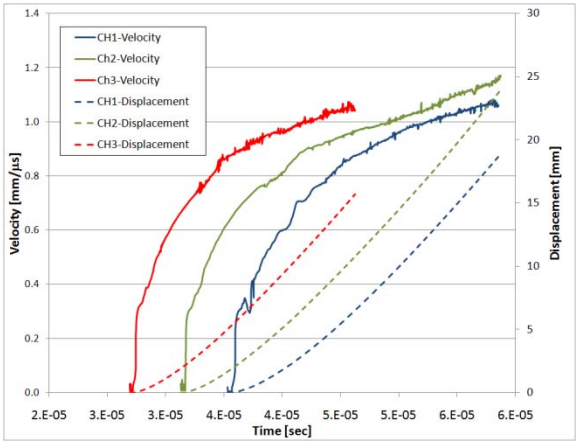

Figure 15. PDV probe traces for ES-1 cylinder experiment

Fig. 15 indicates the velocity (solid lines) and displacement (dashed lines) of three distinct locations along 7.62 mm from the bottom of the cylinder). Channels 2 and 3 are respectively located 2.54 cm and 5.08 cm above Channel 1. A slight increase in noise began approximately 5.5 µs after the wall began expanding (32.3 µs absolute time in Fig. 15). This noise corresponds to a 2.64 mm displacement, or approximately 10.3% increase in the cylinder's diameter. The noise may have arisen from decreased light return as the angle between the probe and cylinder increased and the case began fracture. A longer period of usable data was observed at probe locations lower on the cylinder, indicating that gas products from the booster train (shown at th the cylinder wall as a function of time. In this case, channel 1 corresponds to the bottommost probe (located e top of Fig. 15 prematurely clouded the area of interest. A relative increase in the observed case wall velocities at probe locations 1 and 2 at an absolute time of 55 µs as shown on Fig. 15 indicate that this late-time data may not be reliable because there is no physical explanation for this difference.

CONCLUSIONS

A series of explosively driven cylinder expansion tests were conducted in two different configurations. A tall cylinder configuration led to a plane strain condition in the failure of ES-1 steel case materials explosively driven to failure. While optical records obtained with a framing camera did not prove very useful (due to limitations in spatial and temporal resolution), a PDV system provided a wealth of information. Future tests in this open air configuration will use a dual-instrumented PDV/VISAR configuration and focus on early time shock transition and reflection phenomenon. Additionally, reconfigured probe mounts will be designed to account for the Taylor angle of the expanding cylinder. To compliment continued open-air ES-1 testing, further water catch tank testing of ES-1 rings will be conducted. The present study examined only the Aero-224 tungsten rings in a plane-strain condition. A 25-ring stack of Aero-224 rings was driven to failure with remarkable success in water recovery of the fragments. All steel and tungsten fragments were weighed. Strain measurements were accomplished for tungsten fragments while steel fragments proved very difficult to accurately characterize with any reasonable degree of certainty. The design for the water catch tank provides for a reliable, reproducible and cost-effective method of catching a large number of fragments for subsequent analysis and characterization.

ACKNOWLEDGMENTS

The authors must give credit and appreciation to Lawrence Livermore National Laboratory, US Dept. of Energy, colleagues of D.M. Goto, T.J. Orzechowski, and their range crew for their substantial contribution of information, drawings and advice. Also, acknowledgment is made to the technicians at the Advanced

Warheads Experimentation Facility, AFRL/RWMW for their insight and technical contributions as well as persistence and diligence in conducting experiments and characterizing fragments. Furthermore, the support of E.J. Welle and T.A. Ager of AFRL/RWMF was instrumental in obtaining PDV data.

REFERENCES

1. D.E. Lambert, M.H. Hopson, J.M. Weiderhold. “Dynamic Fragmentation Experiments Under Plane Strain and Uniaxial Stress Conditions,” *Proc. 2010 PVP Conference*, Bellvue, WA, Jul 2010.

2. M.H. Hopson, D.E. Lambert, J.M. Weiderhold. “Computational Comparisons of Homogeneous and Statistical Descriptions of Steel Subjected to Explosive Loading,” *Proc. 2010 PVP Conference*, Bellvue, WA, Jul 2010.1.

3. Defense Special Weapons Agency, “Design and Analysis of Hardened Structures to Conventional Weapons Effects,” DSWA DAHSCWEMAN-97, December 1997, p. 6-5.

4. N.F. Mott. Fragmentation of shell cases. Proc. Royal Soc. London 1947; 189: 300-308.

5. G.I. Taylor. Analysis of the explosive of a long cylindrical bomb detonated at one end. Scientific Papers of G.I. Taylor, Vol. III No. 30. Cambridge University Press, 1963, p 277-286.

6. D.E. Grady, M. M. Hightower. Natural Fragmentation of exploding cylinders. In: Meyers MA, Murr LE, Staudhammer KP, editors. Shock Wave and High-Strain Rate Phenomena in Materials. New York: Marcel Dekker, Inc. 1992. p 713-720.

7. G.I. Taylor. The fragmentation of tubular bombs. Scientific Papers of G.I. Taylor, Vol. III No. 44. Cambridge University Press, 1963, p. 387-390.

8. T.J. Vogler et al., “Fragmentation of Materials In Expanding Tube Experiments,” Intl. J. Impact Engineering XXIX, pp. 735-746.

9. D.M. Goto et al., “Investigation of the Fracture and Fragmentation of Explosively Driven Rings and Cylinders,” Intl. J. Impact Engineering XXXV (12), pp 1547-1556.

10. K.L. Torres et al., “Dynamic Experiments for a High-Strength Experimental Steel,” J. Pressure Vessel Tech. CXXXI no. 2, April 2009.

11. S.J. Bless et al., “Dynamic Fracture of tungsten heavy alloys,” Intl. J. Impact Engineering XXXIII, pp 100-108.

12. G. R. Johnson and W.H. Cook, “A constitutive model and data for metals subjected to large strains, high strain rates, and high temperatures,” *Proceedings of the Seventh International Symposium on Ballistics*, April 1983, pp 541-547.

13. E.L. Lee, H.C. Hornig, J.W. Kury, “Adiabatic Expansion of High Explosive Detonation Products,” Lawrence Radiation Laboratory Report, May 2, 1968.

14. R.W. Gurney. The initial velocity of fragments from bombs, shells, and grenades. *Army Ballistic Research Laboratory Report* No. 405, 1943.

15. W.C. Davis et al., “Explosive-Driven Shock Waves in Argon,” Proc. 13th International Detonation Symposium, 2006.

16. T. Strand et al., “Factors to Consider when Choosing a Probe for PDV,” LLNL-CONF-406957, presented at the 3rd Annual PDV Conference, Sep 2008.

CHAPTER 3

Proceedings of the 2010 Pressure Vessels and Piping Conference

PVP-2010

July 18-22, 2010, Bellevue, Washington, USA

PVP2010-25330

Computational Comparisons of Homogeneous and Statistical Descriptions of Steel Subjected to Explosive Loading

Michael V. Hopson
Naval Surface Warfare Center
Dahlgren Division
Dahlgren, VA, USA

David E. Lambert
Air Force Research Laboratory
Munitions Directorate
Eglin Air Force Base, FL, USA

1st Lt Joseph Weiderhold
Air Force Research Laboratory
Munitions Directorate
Eglin Air Force Base, FL, USA

ABSTRACT

Experiments were conducted by the Munitions Directorate at the Air Force Research Laboratory to investigate the fracture and fragmentation of two different metals due to explosive loading. The first metal, Eglin Steel 1 (ES-1), was a high strength steel alloy configured as a thin shell surrounding the explosive core. The second metal, Aero 224, was a tungsten alloy configured as a stack of rings around the explosive core. The two different configurations generated two different stress states, plane-strain and uniaxial stress. The radial expansion velocity of the ES-1 shell was recorded via a photonic Doppler velocimeter (PDV). Also, the fragments from the ES-1 shell test and Aero 224 ring test were soft captured in a water tank.

Complementary computational analysis was conducted at the Naval Surface Warfare Center Dahlgren Division. An Eulerian wave propagation code (CTH) and a Lagrangian transient dynamics code (Presto) were used to analyze the stress states of the different configurations

and also investigate the use of statistical compensation on explosive fragmentation. The stress states were examined in the context of stress triaxiality where triaxiality is defined as the ratio of pressure to the Von Mises stress. From the computational analysis both the ES-1 shell test and Aero 224 ring test approached, but did not reach the ideal triaxial values for plane-strain and uniaxial stress. Lastly, parametric calculations were conducted in order to determine the effectiveness of using a statistically compensated Johnson Cook fracture model to simulate the non-homogeneous nature of the ES-1 and Aero 224. While using the model did result in different fragment distributions, all the resulting distributions were less accurate than the baseline homogeneous calculation. Scrutiny of the early time fragment formation in the statistically compensated calculations revealed a mesh bias which caused material failure on surfaces parallel to the Cartesian axes. This preferential fracture produced rarefaction waves which prohibited further fragmentation thus generating fragment distributions larger than those observed in the Aero 224 ring test. Potential solutions for this issue will be explored in the future.

INTRODUCTION

The fracture and fragmentation of metals subjected to explosive loading is a topic of continuing interest to the Department of Defense (DOD). Both the underlying physics and the development of predictive tools continue to be investigated. Many people have advanced this topic, but two British physicists, N.F. Mott and G.I. Taylor made fundamental contributions during and shortly after World War II [i,ii]. Somewhat later, that work was expanded upon by D.E. Grady [iii]. More recently, researchers such as T.J. Vogler, D. Goto and R.M. Brannon have made use of more sophisticated diagnostics and computational tools to further probe the complex shock physics that occur under explosive loading [iv,v,vi]. The early work by Mott and Taylor used purely analytical techniques whereas D.E. Grady used both analytical expressions and contemporary numerical codes. A key feature of D.E. Grady's work uses statistical equations to address the observation that metals have a microstructure which leads to non-homogeneous material properties. The role of non-homogeneity continues to be a focus for the current research.

Computational continuum codes can provide many details on the response of metals to explosive loading. However, most "production" level calculations use a homogeneous description of the metal. This is an incorrect representation since metals possess a microstructure whose details create variations in material strength and other properties such as strain to failure. Ultimately these variations influence the formation of fragments at the macroscopic level. The spatial scale of the microstructure is on the order of micrometers and is not readily accessible to current computational tools and resources for system level calculations. Rather than explicitly model the microstructure one can attempt to simulate the effects of material non-homogeneity through the use of a statistical description. Specifically, a statistically compensated Johnson-Cook fracture model has been implemented into the Eulerian shock physics code, CTH [vii]. The model allows the user to define an initial distribution of failure strains which are then used in the Johnson-Cook fracture model.

Two metals, Aero 224 and ES-1 were explosively loaded in a series of tests conducted at Eglin Air Force Base. The Aero 224 is an alloy composed of tungsten particles in a nickel/cobalt matrix. The ES-1 is a high strength steel developed at Eglin Air Force Base. The details of the materials, the tests and the results are specified in companion paper, but a brief summary follows here [viii]. The fragments were soft captured using a water tank and a photonic Doppler velocimetry (PDV) provided the expansion velocity of the ES-1 shell. The Aero 224 is a tungsten alloy and was configured as a stack of rings. However, the ES-1 test used a thin walled shell. The rings generated uniaxial stress and the thin walled shell provided plane-strain. Given this data, the computational analysis of the fragmentation had two goals. First, the results from calculations were used to analyze the stress states from the two different configurations. Second, the distribution of initial failure strains was varied parametrically in order to determine the accuracy of this technique in comparison to typical homogenous calculations.

TEST DESCRIPTION

Both test configurations used an axisymmetric cylindrical stack. The main charge consisted of an aluminized PBX explosive surrounded by the metals under investigation. In both configurations the main charge was initiated by a booster explosive, Composition B, located at one end. At the very top of the assembly an RP-1 initiator was used to detonate the Comp B booster charge. The configuration and test article for Aero 224 are shown in Figure 14. There were 25 Aero 224 rings located in the center of the configuration in between two copper sleeves. The copper sleeves provided confinement for the explosive charge on either side of the Aero 224 rings.

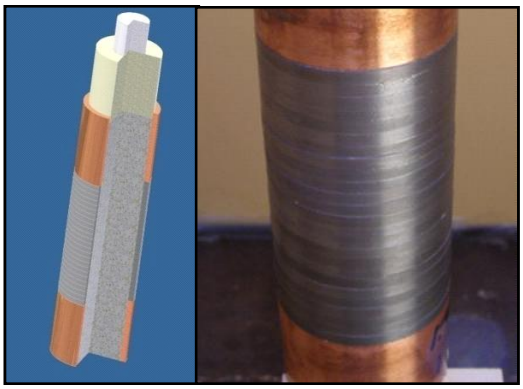

Figure 14 Aero 224 test article CAD drawing (left) and photograph (right)

The main explosive charge was 20.32 cm in length and 5.08 cm in diameter. The Aero 224 rings were 0.4cm wide and tall and the total length of the stack was 10.16 cm. The copper tubes on either side were 5.08 cm in length and were 0.4 cm thick. The configuration for the ES-1 tests was identical except that the Aero 224 rings were replaced by the ES-1 shell. As with the rings, the ES-1 shell was 0.4 cm thick.

STRESS STATE ANALYSIS

As mentioned previously, the computational code CTH was used to analyze the results from the fragmentation tests. CTH is an Eulerian wave propagation code whose numerical framework and materials models are appropriate for high deformation, high strain rate problems. In CTH, the stress tensor is split into the spherical and deviatoric components. This assumes that the spherical or volumetric response is uncoupled from the deviatoric response. That assumption is true for the metals in this analysis.

The pressure volume response is modeled with an equation of state (EOS) which expresses the pressure as a function of other thermodynamic state variables. A Mie-Gruneisen EOS was used for the ES-1 and an analytical EOS from the CTH database for a tungsten alloy was chosen for the Aero 224 [ix]. The deviatoric response for both metals was modeled with a Johnson Cook (JC) strength model [x]. The JC strength parameters were determined from material tests conducted at Eglin Air Force Base and are shown below in Table 2.

Table 2 Johnson Cook strength properties

Material	A (dynes/cm^2)	B (dynes/cm^2)	n	C	m	T* (eV)
ES-1	1.379e10	1.0342e10	0.33	0.02	1.5	0.1465
Aero224	7.929e09	0.0	0.70	0.09	1.20	0.1485

Before proceeding with the stress state analysis the explosive and material models for ES-1 were validated using the photon Doppler velocimetry (PDV) data. The PDV provided the expansion velocity of the expanding ES-1 shell. In this case the PDV recorded the velocities at two points on the cylinder. Since the test article was axisymmetric, it was possible to run the CTH calculation as a 2-dimensional (2D) axisymmetric problem. A 2D computational domain is computationally efficient, but has geometric limitations. The out-of-plane stress component (z) is a function of the in plane components. The material cannot fail in the z direction, so the numerical solution becomes inaccurate for problems where the material does fail out of plane. The goal of this 2D calculation was to validate the explosive model and the ES-1 strength model.

The calculation result is shown in Figure 15. The figure shows a cutaway of the test configuration where pressure contours are superimposed over a plot of the different materials. The units for the pressure contours are in dynes/cm^2. The RP-1 initiator was not explicitly modeled. Instead, the Composition B booster was modeled using a programmed burn model and initiated at the top of the booster. As can be seen in Figure 15 this resulted in a detonation wave that propagated down the length of the cylinder. The right side of the figure shows the detonation at 20 microseconds.

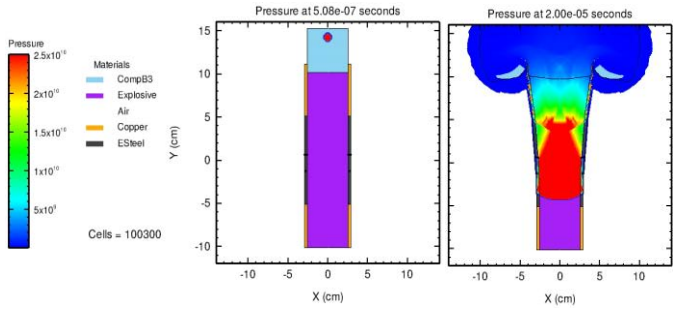

Figure 15 ES-1 2D Axisymmetric Calculation

Time history information was recorded in the CTH calculation at the same locations as the PDV probes. The comparison between the CTH calculation and the PDV test data is shown in Figure 16. Note that the CTH results were arbitrarily aligned in time with the test data. This was necessary due to the simplification regarding the RP-1 initiator. The calculation matched the initial radial expansion of the ES-1 shell closely. However, between 40 and 50 microseconds the calculations results diverged from the PDV data. In the test, explosive gases would have started flowing between cracks in the shell. This would have reduced the interior pressure resulting in a lower radial expansion velocity. The 2D axisymmetric CTH calculation was incapable of fracturing in the Z direction, so the interior pressure remained high causing the divergence with the PDV data. Given the good match, the explosive model parameters and ES-1 strength parameters were used in subsequent analysis.

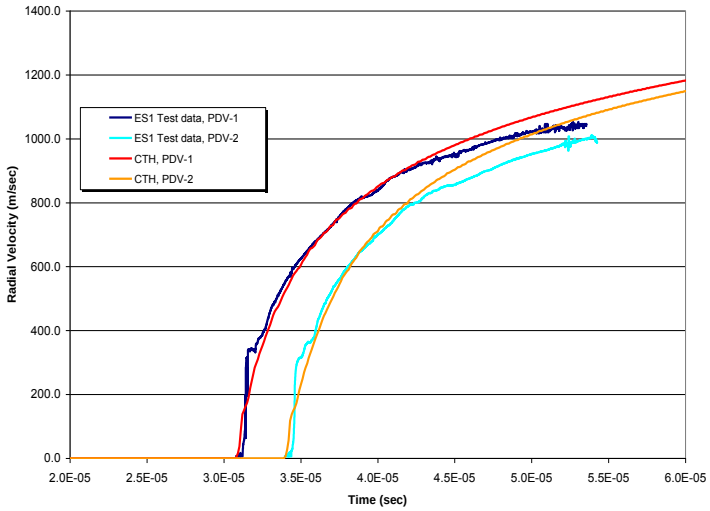

Figure 16 ES-1 PDV Test Data Comparison

Triaxiality is defined as the ratio of pressure to Von Mises stress. It is a convenient metric for defining the load path. In this analysis, pressure was positive and tension was negative. The triaxiality was calculated by recording the stresses in a ring located in the center of the test article. The triaxiality for the Aero 224 ring is shown in Figure 17. The detonation wave arrived at ~15 microseconds resulting in deformation of the Aero 224 ring. The expansion generated deviatoric stress in the Aero 224 ring. The triaxiality fluctuated due to shock

interactions within the ring but approached a tensile dominated stress state as the ring expanded. In a pure uniaxial stress state the triaxiality is -0.33. Note that the calculation only reached a value of ~ -0.20.

In addition to the triaxiality, the material damage was also plotted in Figure 17. The Johnson Cook (JC) fracture model was used to determined material failure. This model is discussed in more detail under the fragmentation analysis. The JC fracture model uses a scalar damage variable where 0.0 is the undamaged state and 1.0 is a fully failed material. As the Aero 224 expanded it accumulated more material damage until it fully failed. Note that as the material approached failure it became unable to support deviatoric stress. Therefore, the Von Mises stress became undefined, resulting in fluctuations in the triaxiality.

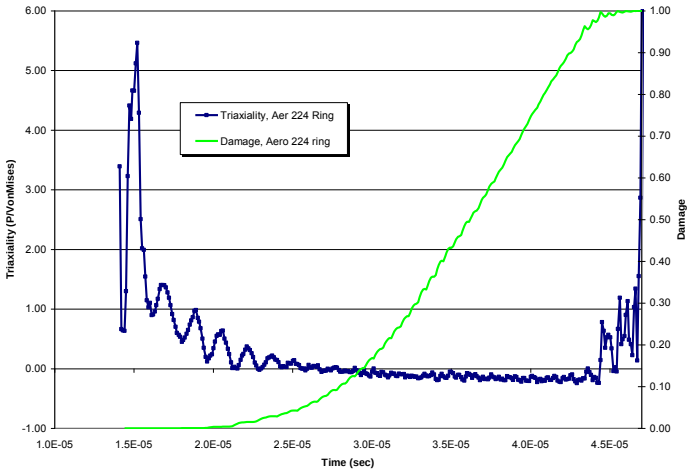

Figure 17 Aero 224 Ring Triaxiality and Damage

The triaxiality was calculated by recording the stresses in the middle of the ES-1 shell halfway along the length of the shell. As before, the detonation wave reached the recording point at ~15 microseconds. The shell configuration approximates a plane-strain condition. The triaxiality for pure plane-strain is -0.577. Prior to becoming undefined the triaxiality from the calculation reached -0.37.

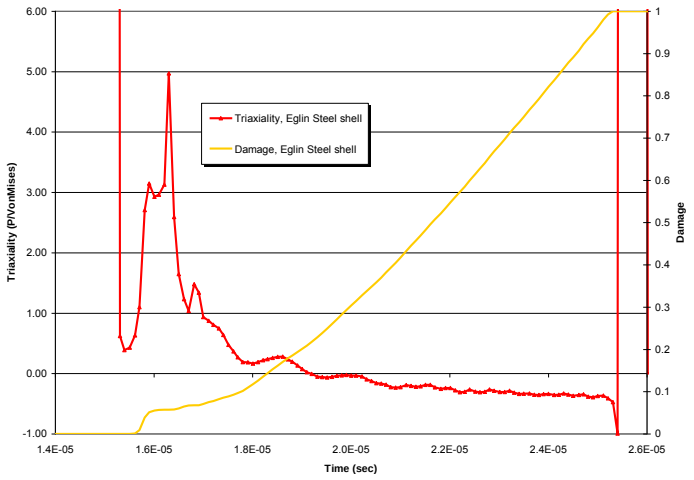

Figure 18 ES-1 Shell Triaxiality and Damage

FRAGMENTATION ANALYSIS

A much more complete analysis of the triaxiality in both the ES-1 and WHA tests can be found in a companion paper [xi]. However, the focus of this effort was to investigate fragmentation. In order to run fragmentation calculations a full 3-dimensional (3D) domain was required. The 3D domain allows for the formation of fragments. However, it is also computationally expensive. The following calculations each took approximately 20000 cpu-hours compared to approximately 4 cpu-hours for the 2D calculations. A cutaway of an Aero 224 calculation is shown in Figure 19. Pressure contours in dynes/cm^2 are superimposed over the materials. Note that while the actual Aero 224 test had 25 rings, the calculations only had 3 rings. The spatial resolution required to capture the fragmentation was approximately 0.03 cm. In order to reduce computational expense, only 3 rings were specified. In later analysis, the fragment distributions were normalized in order to compare the computational results to the test data.

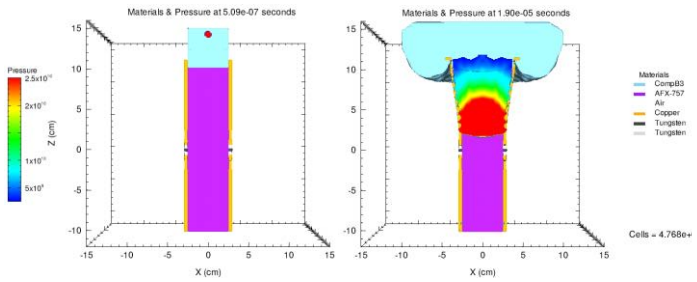

Figure 19 Aero 224 Ring Fragmentation Calculation

The Johnson-Cook (JC) fracture model uses a scalar damage equation for predicting failure of materials [xii]. The material fails when the damage parameter, D, reaches unity. The strain to

fracture ε_F parameters include equivalent plastic strain rate ε_{Dot}, pressure P, constants D1 through D5, the local yield stress Y, and the homologous temperature T_{HOM}. The homologous temperature is calculated from the current temperature T, the room temperature T_{Room} and the melting temperature T_M. Initial failure strain ε_{F0} can be varied using a Weibull statistical distribution function if desired. The Weibull distribution is used to simulate subgrid physics such as microstructure or adiabatic shear banding.

$$D = \int \frac{\varepsilon_{Dot}}{\varepsilon_F} dt \quad \textbf{(1)}$$

$$T_{HOM} = (T - T_{Room}) / (T_M - T_{Room}) \quad \textbf{(2)}$$

$$\varepsilon_{F0} = (D1 + D2) \quad \textbf{(3)}$$

$$\varepsilon_F = \left(\varepsilon_{F0} - D_2\left(1 - e^{-D_3 * p/Y}\right)\right) * \left(1 + D_4 * \ln\left(\frac{\varepsilon_{Dot}}{\dot{\varepsilon}_{ref}}\right)\right) * \left(1 + D_5 * T_{HOM}\right) \quad \textbf{(4)}$$

The Weibull cumulative distribution function (CDF) and the probability density function (PDF) are provided in equations 5 and 7 respectively where the parameters include the scale factor a, modulus m, and failure strain ε. The values for the parameters used in the JC fracture model for the computational analysis are shown in Table 3 and were taken from the CTH database for pure tungsten [ix].

Table 3 Johnson Cook fracture model parameters

Material	D1	D2	D3
Aero224	0.0	0.33	-1.50

In the current analysis, the modulus value for the Weibull compensated JC fracture model was varied to determine its affect on the predicted fragment mass distribution. The sum of the JC fracture model constants, D1 and D2, equals the initial failure strain. However, with this approach the initial failure strain is also the mean of the failure strain **distribution. Three** different Weibull moduli (2, 6 and 10) were investigated to provide a range of distributions from broad to more narrow.

$$C_F = 1 - e^{[-\phi(\varepsilon)]} \quad \textbf{(5)}$$

$$\phi(\varepsilon) = \left(\frac{\varepsilon}{a}\right)^m \quad \textbf{(6)}$$

$$P_F = \frac{m}{a}\left(\frac{\varepsilon}{a}\right)^{m-1} e^{\left[-\left(\frac{\varepsilon}{a}\right)^m\right]} \quad \textbf{(7)}$$

Results from different Aero 224 fragmentation calculations are shown in Figure 20. Only the Aero 224 ring from the center is shown with the view along the Z-axis. Moving from left to right, a wider range of initial failure strains were introduced into the calculations. From the figure it can be seen that applying a distribution of initial failure strains in the JC fracture model had little influence on the breakup of the Aero 224 ring.

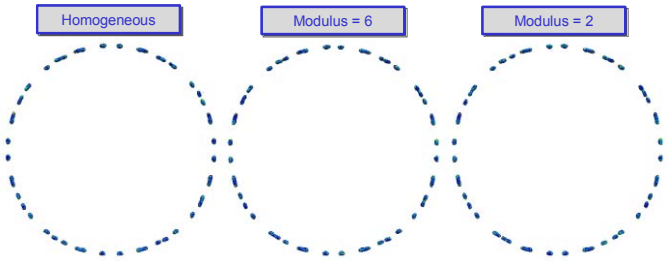

Figure 20 Aero 224 Ring Parametric Calculation Results

The cumulative fragment distributions from the parametric analysis are compared against the test data in Figure 21. The cumulative mass was plotted against the fragment mass. The results were normalized so that the computational results could be compared to the test data. The fragment distribution from a homogeneous representation of the Aero 224 produced the most accurate solution. Application of different Weibull distributions produced slightly less accurate solutions.

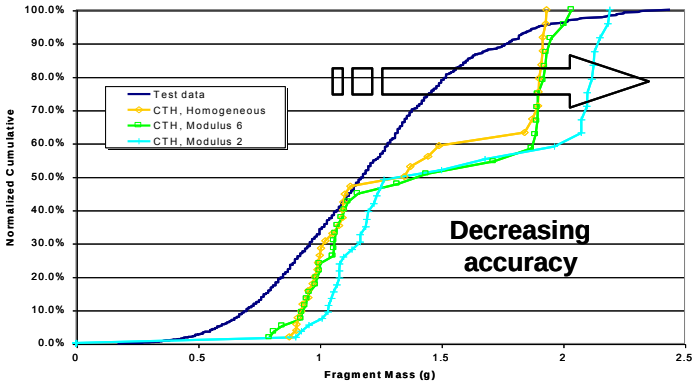

Figure 21 Parametric CTH Calculation Comparison

This result contradicted earlier analysis of an explosively loaded shell [xiii]. CTH is a multi-material Eulerian code and as such is subject to advection errors. An advection error is where the advection of material through the computational mesh can cause material model parameters to degrade. Several heuristic features can influence this degradation including material interface reconstruction. Typically, higher resolution meshes are used to minimize this effect. In order to quantify the advection error on the initial distribution of failure strains a moving ring calculation was conducted. Figure 22 shows a calculation where a metal ring was translated from left to right at a velocity of 1 cm/μs. The black lines show the adaptive mesh where each block contains 10 x 10 computational cells.

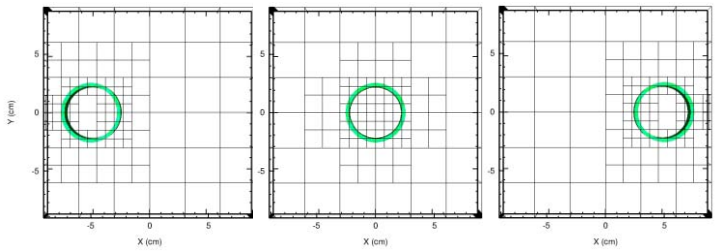

Figure 22 Moving Ring Calculation

In this calculation an initial distribution of failure strains using a Weibull modulus of 10 was assumed. A plot of the Weibull probability density function is shown in Figure 23. Also shown are the initial failure strain distributions from the moving ring CTH calculation. Note that over time, the distribution narrowed. This error would tend to mitigate the effect of varying the Weibull modulus.

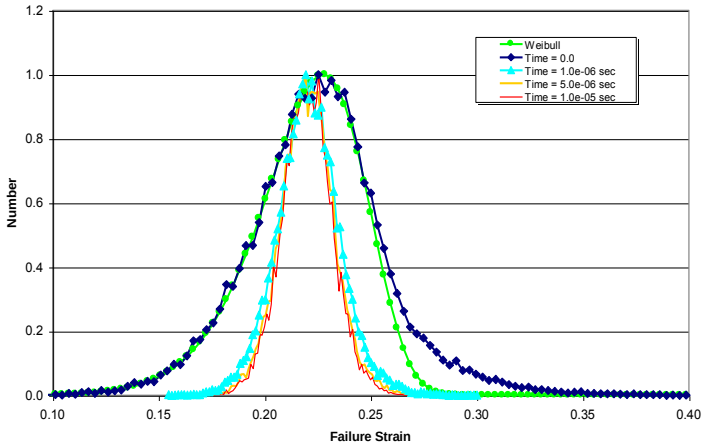

Figure 23 Influence of Advection on Failure Strain Distribution

Lagrangian codes do not advect material and so do not suffer from advection error. Therefore, it was thought that a Lagrangian code might produce a more accurate answer. With this in mind, Presto, a transient dynamics Lagrangian code developed by Sandia National Lab was used to calculate the break up of the Aero 224 ring [xiv]. A fully coupled calculation between CTH and Presto was possible. However, in the interest of time a simpler, loosely coupled calculation was used instead. The blast pressure from the 2D CTH calculation was used to drive the expansion of an Aero 224 ring. The Presto calculation used the same material models and parameters as the CTH calculation. Furthermore, the Presto calculation included only a single Aero 224 ring. The results of the Presto calculation using a Weibull modulus of 2 are shown in Figure 24. The color contours show the level of Johnson Cook fracture model damage.

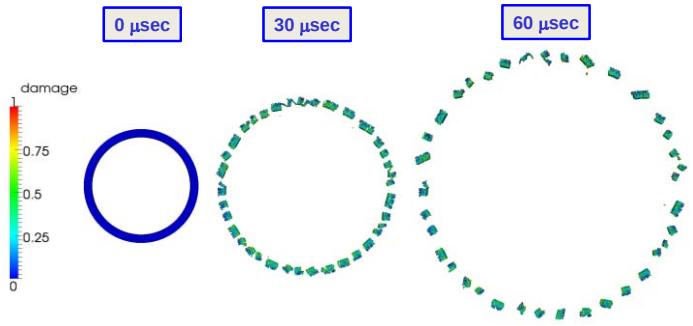

Figure 24 Presto Calculation of Aero 224 Ring

The fragment distribution from the Presto calculation differed markedly from the CTH results. A photo of the Aero 224 fragments is shown in Figure 25 and it can be seen that the fragment shapes from the Presto calculation qualitatively resemble the actual fragments

recovered from the test. More importantly, the same figure shows the quantitative comparison of the normalized cumulative fragment distribution for different Weibull moduli. Varying the Weibull modulus in the Presto calculation did result in different fragment distributions. The most accurate solution was produced using a Weibull modulus of 4. In that calculation, the mean fragment size was 0.98 gm compared to 1.05 gm from the test data.

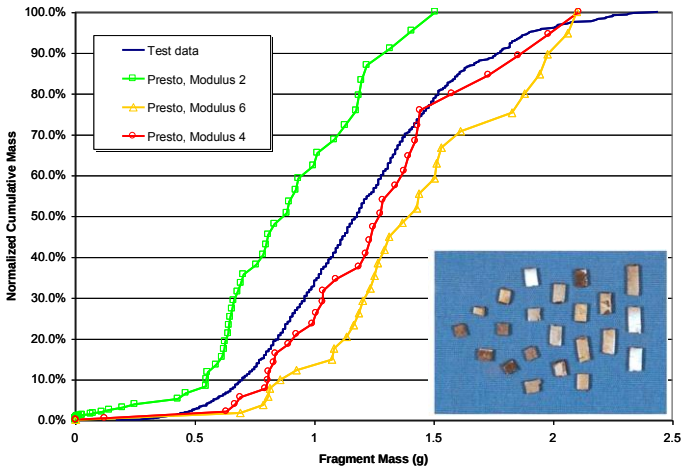

Figure 25 Parametric Presto Calculation Comparison

The Presto calculations demonstrated a capability to modulate the fragment size distribution using a Weibull compensated JC damage model. While this was a positive achievement, it was still a deterministic result. It is possible to vary the random seed used to determine the distribution of initial failure strains. A stochastic analysis could be conducted by using many seed values. Another limitation of this analysis was the use of a loosely coupled approach for the Presto calculations. A fully coupled approach could be employed in the future to determine the error associated with the loosely coupled approach.

CONCLUSION

Experiments were conducted at Eglin Air Force Base to investigate explosively driven fragmentation with particular attention given to material triaxiality. Complementary computational analysis used the Eulerian wave propagation code, CTH, to analyze the stress states and fragmentation of those experiments. The 2D axisymmetric calculations were able to match the radial expansion velocity of the ES-1 test. This provided confidence in the subsequent analyses. The triaxiality of the Aero 224 ring test and ES-1 shell test were calculated. Both scenarios began with high compressive triaxiality and then progressed into tensile stress states. The Aero 224 calculation reached a triaxiality of -0.20 compared to the ideal value of -0.33 for uniaxial stress. The ES-1 calculation reached a triaxiality of -0.37 compared to the ideal value of -0.57 for 2D plane-strain.

Typical continuum code calculations assume that the material properties of a metal are homogeneous. This assumption is incorrect and generates errors in fracture and fragmentation calculations. In an effort to improve on this assumption, a statistically compensated JC fracture model was implemented in the Eulerian wave propagation code, CTH. A parametric analysis was conducted in order to determine the effect of varying the distribution of initial failure strains on the fragmentation of the Aero 224 rings. Varying the Weibull modulus had a minimal effect on fragment mass distributions,

Since this contradicted earlier analysis, the cause for the behavior was investigated. Analysis of the distribution of initial failure strains revealed that advection error caused the Weibull distribution to change over time. A loosely coupled calculation using the blast pressure from CTH to drive the expansion of the Aero 224 ring in the Lagrangian code, Presto, produced a more accurate solution. Using a Weibull modulus of 4, the average fragment mass was 0.98 gm compared to 1.05 gm from the test data.

ACKNOWLEDGMENTS

The author thanks Tracy Vogler, Dana Goto, and Dennis Grady for their generosity with both test data and advice on high strain rate fragmentation. The author also thanks Bert Meyer and Rebecca Brannon for developing a Weibull compensated Johnson Cook fracture model in the CTH code.

REFERENCES

Mott NF, Fragmentation of shell cases, Proc. Royal Soc. London A 1947, 189: 300-308.
Taylor GI, Analysis of the explosive of a long cylindrical bomb detonated at one end. Scientific Papers of G.I. Taylor, Vol. III No. 30, Cambridge University Press, 1963, p 277-286.
Grady DE, “Fragmentation of Rings and Shells: The Legacy of N.F. Mott”, Springer Verlag, 2006.
Vogler TJ et al, Fragmentation of Materials In Expanding Tube Experiments, Intl. J. Impact Engineering XXIX, pp. 735-746, December 2003.
Goto DM et al, Investigation of the Fracture and Fragmentation of Explosively Driven Rings and Cylinders, Intl. J. Impact Engineering XXXV (12), pp 1547-1556, December 2008.
Brannon RM, JM Wells, OE Strack, Validating Theories for Brittle Damage, Minerals, Metals and Materials Society, Volume 38A, 28 September 2007, Published online.
Hertel Jr. ES, RL Bell, MG Elrick, AV Farnsworth, GI Kerley, JM McGlaun, SV Petney, SA Silling, PA Taylor, and L Yarrington, CTH: A Software Family for Multi-Dimensional Shock Physics Analysis, Proceedings of the 19th International Symposium on Shock Waves, Volume I, pages 377-382, Marseille, France 26-30 July 1993.
Weiderhold J, DE Lambert, MV Hopson, Experimental Design and Data Collection for Dynamic Fragmentation Experiments, Proc. 2010 PVP Conf., Bellevue, WA, July, 2010.
Thompson SL, ANEOS Analytic Equations of State for Shock Physics Codes Input Manual, Sandia National Lab Report SAND89-2951, Albuquerque, NM, March, 1990.
Johnson GR, WH Cook, A Constitutive Model and Data for Metals Subjected to Large Strains, High Strain Rates and High Temperatures, Seventh International Symposium on Ballistics, Hague, Netherlands, April, 1983.

Lambert DE, J Weiderhold, J Osborn, MV Hopson, Dynamic Fragmentation Experiments Under Plane Strain and Uniaxial Stress Conditions, to be published in Proc. 2010 PVP Conf, Bellevue, WA, July 2010.
Johnson GR, WH Cook, Fracture Characteristics of Three Metals Subjected to Various Strains, Strain Rates, Temperatures and Pressures, Eng Fract Mech 1985; 21(1):31-48.
Hopson MV, CM Scott and R Patel, Computational Comparisons of Homogeneous and Statistical Representations of AerMet 100 Subjected to High Strain Rate Loading, 11th Hypervelocity Impact Symposium, Freiburg, Germany, April 2010.
Presto 4.14 User‟s Guide, SIERRA Solid Mechanics Team, Engineering Sciences Center, Sandia Report 2009-7410, Sandia National Laboratories, Nov. 2009.

Distribution List

AFRL-RW-EG-TR-2010-106

Defense Technical Information Center 8725 John J. Kingman Road, Ste 0944 Ft Belvoir, VA 22060-6218	1 Electronic Copy (1 file, 1 format)
EGLIN AFB OFFICES:	
AFRL/RW CA-N	(Provided notice of publication only)
AFRL/RWOC (STINFO Office)	1
AFRL/RWME	1
AFRL/RWMF	1
AFRL/RWMW	1
AFRL/RWPC	1